Published in final edited form as:

Neuron. 2017 December 06; 96(5): 1055–1069.e6. doi:10.1016/j.neuron.2017.10.025.

The Wnt Inhibitor Apcdd1 Coordinates Vascular Remodeling and Barrier Maturation of Retinal Blood Vessels

Jenna Mazzoni[1,5], **Julian R. Smith**[1], **Sanjid Shahriar**[1,2], **Tyler Cutforth**[1,4], **Bernardo Ceja**[5], and **Dritan Agalliu**[1,2,3,4,6,*]

[1]Department of Neurology, Columbia University Medical Center, New York, NY 10032, USA

[2]Department of Pathology & Cell Biology, Columbia University Medical Center, New York, NY 10032, USA

[3]Department of Pharmacology, Columbia University Medical Center, New York, NY 10032, USA

[4]Columbia Translational Neuroscience Initiative, Columbia University Medical Center, New York, NY 10032, USA

[5]Department of Developmental and Cell Biology, University of California, Irvine, CA 92697, USA

SUMMARY

Coordinating angiogenesis with acquisition of tissue-specific properties in endothelial cells is essential for vascular function. In the retina, endothelial cells form a blood-retina barrier by virtue of tight junctions and low transcytosis. While the canonical Norrin/Fz4/Lrp5/6 pathway is essential for angiogenesis, vascular remodeling, and barrier maturation, how these diverse processes are coordinated remains poorly understood. Here we demonstrate that Apcdd1, a negative regulator of Wnt/β-catenin signaling, is expressed in retinal endothelial cells during angiogenesis and barrier formation. *Apcdd1*-deficient mice exhibit a transient increase in vessel density at ages P10–P12 due to delayed vessel pruning. Moreover, *Apcdd1* mutant endothelial cells precociously form the paracellular component of the barrier. Conversely, mice that overexpress Apcdd1 in retina endothelial cells have reduced vessel density but increased paracellular barrier permeability. Apcdd1 thus serves to precisely modulate Wnt/Norrin signaling activity in the retinal endothelium and coordinate the timing of both vascular pruning and barrier maturation.

INTRODUCTION

Forming a functional vertebrate vascular network requires coordination of tissue-specific angiogenesis with endothelial cell (EC) differentiation, so that vessels adopt the specialized

*Correspondence: da191@cumc.columbia.edu.
[6]Lead Contact

SUPPLEMENTAL INFORMATION

Supplemental Information includes six figures and can be found with this article online at https://doi.org/10.1016/j.neuron.2017.10.025.

AUTHOR CONTRIBUTIONS

J.M., J.R.S., T.C., and D.A. designed all experiments, J.M., J.R.S., T.C., S.S., B.C., and D.A. performed the experiments and analyzed the data, and J.M., T.C., J.S., S.S., and D.A. wrote the manuscript.

functions appropriate to the organs they subserve (Adams and Alitalo, 2007; Potente et al., 2011). In the murine central nervous system (CNS), angiogenesis is tightly coordinated with the acquisition of EC barrier properties, known as the blood-brain barrier (BBB), that prevent free diffusion of molecules between the blood and the CNS (Chow and Gu, 2015; Zhao et al., 2015). Brain angiogenesis occurs during both embryonic and postnatal development, when ECs invade the neuroepithelium from the perivascular plexus, whereas retinal angiogenesis occurs exclusively at postnatal stages, with ECs from the brain invading the optic nerve (Mancuso et al., 2008; Stahl et al., 2010). During vessel development, CNS ECs tightly coordinate angiogenesis with both vessel pruning and formation of a functional barrier. The latter features three unique properties: (1) presence of tight junction (TJ) proteins that limit paracellular permeability between ECs, (2) a low rate of receptor-mediated endocytosis (transcellular permeability), and (3) expression of transporter proteins to facilitate bidirectional transport of molecules across the endothelium (Klaassen et al., 2013; Obermeier et al., 2013). Although CNS angiogenesis and barrier maturation are tightly coordinated, the mechanisms through which this is achieved remain unclear.

The Wnt/β-catenin pathway controls both CNS angiogenesis and barrier development (Daneman et al., 2009; Liebner et al., 2008; Stenman et al., 2008; Zhou et al., 2014). Canonical Wnts regulate vascular morphogenesis through stabilization and translocation of β-catenin into the nucleus to induce the transcriptional targets that control angiogenesis, proliferation, survival, and barrier formation (Dejana, 2010). While angiogenesis and barrier formation in most brain regions are promoted by activation of β-catenin through the Wnt-7a/b/Frizzled/Lrp5/6 ligand-receptor complex, in the retina and cerebellum these functions are provided by the related Norrin/Frizzled-4/Lrp5/6 signaling module (Wang et al., 2012; Ye et al., 2009; Zhou et al., 2014). Signal specificity is dictated by the presence of obligatory unique co-receptors such as GRP-124/Reck for Wnt-7a/b and Tspan-12 for Norrin (Cho et al., 2017; Junge et al., 2009; Lai et al., 2017). Loss-of-function (LOF) studies for the genes *Ndp* (encoding Norrin), *Frizzled-4* (*Fz4*), *Lrp5/6*, and *Tspan-12* in mouse retinae all show delayed and incomplete growth of the primary vascular plexus as well as loss of deep vascular plexi (Chen et al., 2012; Junge et al., 2009; Luhmann et al., 2005; Xia et al., 2010; Ye et al., 2009; Zuercher et al., 2012). Inhibiting Norrin/Fz4/Lrp5/6 signaling also results in loss of blood-retina barrier (BRB) integrity, indicating that the canonical pathway is essential for BRB formation and maintenance (Paes et al., 2011; Wang et al., 2012). Although Wnt activity is reduced in CNS ECs as they transition from a highly angiogenic to a more quiescent, “barrier-forming” state (Daneman et al., 2009; Liebner et al., 2008; Wang et al., 2012), to date it has not been demonstrated whether distinct levels of Wnt signaling regulate angiogenesis versus remodeling and barrier maturation within retinal ECs.

Adenomatous polyposis coli downregulated 1 (Apcdd1), a membrane-bound glycoprotein with a highly conserved cysteine-rich region in its extracellular domain, is both a downstream target and inhibitor of the canonical Wnt pathway (Shimomura et al., 2010; Takahashi et al., 2002). Apcdd1 was identified as the second-most enriched gene in brain ECs compared to lung and liver endothelium and is uniquely expressed within the CNS vasculature (Daneman et al., 2010a). Moreover, *Apcdd1* mRNA levels decrease in both $Norrin^{-/-}$ and $Lrp5^{-/-}$ retinas, indicating that it is a target for Norrin/Fz4/Lrp5/6 signaling

(Chen et al., 2012). Apcdd1 blocks the interaction between Wnt3A and Lrp5, thus inhibiting downstream stabilization of β-catenin and several Wnt-mediated developmental processes including embryonic axis specification, neural proliferation, and hair follicle formation (Shimomura et al., 2010). These findings suggest that Apcdd1 may be a key regulator of Wnt activity that coordinates CNS angiogenesis and BRB formation.

To determine whether Apcdd1 is required for retinal angiogenesis and barrier formation in the retina, we have generated *Apcdd1*-deficient mice and examined retinal vascular densities during development. While the initial stages of retinal angiogenesis are normal, *Apcdd1*-deficient mice exhibit a transient increase in vessel density between postnatal days 10 and 12 (P10 and P12), due to decreased vessel pruning. Conversely, *Apcdd1*$^{-/-}$ mice display accelerated BRB maturation, as evidenced by decreased paracellular permeability of retinal blood vessels to low-molecular-weight tracers. Primary brain ECs isolated from *Apcdd1*$^{-/-}$ mice also display abnormal paracellular and transcellular barrier properties, suggesting that the gene functions cell autonomously in ECs. Conversely, mice that overexpress Apcdd1 in retinal endothelial cells have reduced vessel density but increased paracellular barrier permeability. These findings provide evidence that Apcdd1 precisely adjusts levels of canonical Wnt signaling to coordinate the timing of vascular pruning with barrier maturation in the developing retina.

RESULTS

Apcdd1 Is Expressed Postnatally in Retinal Blood Vessels

To investigate the function of Apcdd1 in retinal angiogenesis and BRB function, we first determined the expression of *Apcdd1* mRNA from P6 to P17 by RNA *in situ* hybridization. *Apcdd1* mRNA is expressed in the superficial vascular plexus present within the ganglion cell layer (GCL) of the retina at P6 (Figure 1A, white arrow). *Apcdd1* mRNA is also detected in the inner nuclear layer (INL) at P8, when the superficial plexus begins to branch into deeper layers of the retina to form the deep plexi (Figure 1C, white arrows). Retinal vascular expression of *Apcdd1* mRNA persists to P12 and P17 (Figures 1E and 1G, white arrows) and mirrors that of *Claudin-5*, a marker for blood vessels (Figures 1B, 1D, 1F, and 1H). We confirmed expression of *Apcdd1* mRNA in endothelial cells using RNA *in situ* hybridization for *Apcdd1* mRNA coupled with immunohistochemistry for Caveolin-1, an EC marker, in P12 and P17 wild-type retinas (Figures 1I–1L, white arrows). However, *Apcdd1* mRNA has very little co-localization with *PDGFR*β mRNA, a marker for pericytes, by double fluorescent RNA *in situ* hybridization (Figures 1M–1P, S1A, and S1B). *Apcdd1* mRNA is also expressed in other regions of the eye, including the neuroblast layer (NBL) and INL (Figures 1A, 1C, 1E, and 1G; yellow arrows); however, it does not colocalize with *Sox9* mRNA (a Müller glia marker; Figures S1C–S1E) suggesting that neuroglial progenitors or neurons produce *Apcdd1*. These results demonstrate that *Apcdd1* mRNA is present in endothelial cells, but not pericytes, during the establishment of both superficial and deep plexi, as well as in a few other cell types.

Loss of Apcdd1 Leads to a Transient Increase in Vessel Density

To examine whether Apcdd1 affects retinal angiogenesis, we used a previously described *Apcdd1* mutant strain in which loxP sites had been engineered to flank exons 2 and 3 (Figure S2A) (Turakainen et al., 2009). Deletion of these exons introduces a premature stop codon after splicing to terminate translation, resulting in a truncated and presumably non-functional protein. We crossed *Apcdd1Ex2,3*$^{flox/flox}$ mice to a strain bearing the Cre recombinase under a heat shock promoter (Dietrich et al., 2000) to yield *Apcdd1Δex2,3*$^{-/-}$ mutants (Figures S2A and S2B). *Apcdd1Δex2,3*$^{-/-}$ (hereafter designated *Apcdd1*$^{-/-}$) mutants are viable and fertile and do not exhibit any overt embryonic developmental defects. We confimed loss of *Apcdd1* mRNA by RNA *in situ* hybridization with an antisense probe for exons 2 and 3 in *Apcdd1*$^{-/-}$ P12 and P17 retinas (Figures S2C–S2F). As an initial assay, we counted vessel sprouts at the vascular front in wild-type and *Apcdd1*$^{-/-}$ P5 retinas (Figures 2A–2D and 2M). *Apcdd1*$^{-/-}$ retinas show no differences in the number of vessel sprouts or the lengths of the vascular front from the base of the optic cup, as compared to wild-type tissue (Figures 2A–2D and 2M and data not shown). Thus, the initial stage of vessel development, namely angiogenic sprouting, is unaffected by loss of *Apcdd1* function.

We next measured vessel densities at multiple developmental stages, ranging from P5 to P14. *Apcdd1*$^{-/-}$ retinas at ages P10 and P12 have increased vessel density within the perivenous capillary beds at the leading edge of the retinal leaflet compared to those from littermate controls (Figures 2E–2L, white arrows). Vessel density in the retina increases from 38% to 43% at P10 and from 23% to 27% at P12 in *Apcdd1*$^{-/-}$ compared to wild-type littermates (Figure 2N). However, this hypervascularized phenotype is resolved by P14, indicating a transient defect in vascular density. Moreover, *Apcdd1*$^{-/-}$ mice have increased vein diameters at P10 (Figures 2F, 2H, and 2P); however, there was no change in arterial diameter from P8 to P12 (Figure 2O). These data demonstrate that loss of *Apcdd1* causes both a transient increase in vessel density and vein abnormalities within the retina.

Because *Apcdd1* is a target for Norrin/Fz4/Lrp5/6 signaling in retinal blood vessels (Chen et al., 2012), we examined whether the hypervascularization phenotype is due to increased Norrin/Fz4/Lrp5/6 signaling and β-catenin activity in ECs. We measured expression levels of Sox17, a Wnt/β-catenin target gene (Corada et al., 2013; Lengfeld et al., 2017; Zhou et al., 2015), in retinal ECs. *Apcdd1*$^{-/-}$ ECs show increased nuclear Sox17 signal intensity compared to wild-type littermate controls at P10 (Figures S2G–S2J, white arrows, S2K). Moreover, *Apcdd1*$^{-/-}$ P10 retinas showed increased pLRP6/LRP6 and active β-catenin/total β-catenin protein ratios, two markers of active canonical Wnt signaling (Bilic et al., 2007), as compared to wild-type P10 retinas, by quantitative LICOR western blotting (Figures S2L–S2O). These findings are consistent with Apcdd1 functioning as an inhibitor of Norrin/Fz4/Lrp5/6 signaling in retinal ECs and suggest that higher levels of Wnt signaling in ECs are responsible for the hypervascularization defects observed in *Apcdd1*-deficient mice. Because Norrin/Fz4/Lrp5/6 signaling controls development of the deep vascular plexus (Zuercher et al., 2012), we analyzed vascular densities in the deep plexus from P10 to P14 (Figures S3I–S3L and S3N). *Apcdd1*$^{-/-}$ retinas show no significant differences in vessel densities of the deep plexus at any developmental stage compared to wild-type controls (Figures S3I–S3L and S3N). These findings indicate that loss of *Apcdd1* does not affect EC

sprouting from the superficial plexus into the deep layers of the retina or formation of the deep plexi.

Apcdd1 Mutants Undergo Decreased Pruning of Retinal Vasculature

Since Wnt signaling controls EC cell proliferation (Dejana, 2010), the hypervascularized phenotype in *Apcdd1*$^{-/-}$ mice may result from increased EC proliferation following increased Norrin/Fz4/Lrp5/6 activity in retinal ECs (Figures S2G–S2O). We administered 5-ethynyl-2′-deoxyuridine (EdU) at P8, P10, and P12 and measured its incorporation within retinal blood vessels to assess the number of cells in S phase. *Apcdd1*$^{-/-}$ retinas show no significant difference in the number of EdU^{+} ECs at any time point compared to wild-type littermate controls (Figures 3A–3H, yellow arrows, 3Q, and 3R). Therefore, the hypervascularization seen in *Apcdd1* knockout retinas is not due to increased EC proliferation. We also examined whether there was differential survival of *Apcdd1*$^{-/-}$ compared to wild-type ECs by counting the number of cleaved Caspase-3^{+} ECs at P10 retinas. We found no difference between the two genotypes, suggesting that *Apcdd1*$^{-/-}$ ECs undergo a rate of cell death similar to wild-type retinas (Figures S3A–S3D and S3M).

An alternative explanation for increased vessel density could be delayed vessel pruning, a critical developmental stage of vascular remodeling in which ECs in newly formed vessels undergo selective regression to yield the mature vascular plexus (Korn and Augustin, 2015). One indication of vascular remodeling is the emergence of empty extracellular matrix (ECM) sleeves within the capillary network, which contain ECM proteins secreted from ECs and mural cells to stabilize nascent vessels, but lack ECs. To determine whether loss of *Apcdd1* causes a delay in vascular remodeling, we isolated retinas at P10 and P14 and stained for the vascular marker BSL-rhodamine and the ECM protein Collagen IV. *Apcdd1*$^{-/-}$ and wild-type retinas were examined for empty ECM sleeves that are Collagen IV^{+} and BSL-rhodamine^{-} (Figures 3I–3P, white arrows). *Apcdd1* mutant mice have fewer empty ECM sleeves as compared to wild-type littermate controls at P10, but not P14 (Figures 3I–3P and 3S). These data suggest that loss of Apcdd1 delays vessel pruning, resulting in a hypervascularized superficial plexus.

Apcdd1$^{-/-}$ Retinas Produce Neurons and Glia at Normal Levels and Have Normal Pericyte Coverage

Since *Apcdd1* mRNA is expressed in both ECs and neuroglial progenitors (NBL layer) and neurons (INL layer) in the retina, we examined whether loss of *Apcdd1* has any impact on differentiation of neuronal or glial cells. We performed immunofluorescence for several neuronal and glial markers in sections from P10 retinas and quantified cell numbers from both wild-type and *Apcdd1* mutants. Quantification of Isl-1 (amacrine, bipolar, and ganglion cells), rhodopsin (photoreceptors), neurofilament (horizontal cells), and Sox9 (Müller glia) showed that *Apcdd1*$^{-/-}$ retinas have similar numbers of neurons and Müller glia cells as compared to wild-type tissues (Figures S4A–S4L). *Norrin* mRNA levels in the retina (produced primarily by Müller glia) were also similar between the two genotypes (Figures S4M and S4N). Moreover, pericyte coverage was similar between wild-type and *Apcdd1*$^{-/-}$ P14 retinas (Figures S3E–S3H). Therefore, the vascular defects observed in *Apcdd1*$^{-/-}$ retinas are likely due to a cell-autonomous defect in the retinal endothelium rather than a

secondary phenotype arising from a signaling deficit following loss of neurons, Müller glia, or pericytes.

The Paracellular but Not Transcellular Blood-Retina Barrier Develops Prematurely in *Apcdd1* Mutants

Norrin/Fz4/Lrp5/6 signaling is necessary for BRB integrity (Wang et al., 2012; Zhou et al., 2014), prompting us to examine whether loss of *Apcdd1* affects barrier maturation of the developing retinal vasculature. To measure paracellular BRB permeability, we injected the low-molecular-weight tracer 5-(and-6)-tetramethylrhodamine biocytin (biocytin-TMR, 869 Da), which crosses the endothelial barrier when tight junctions are disrupted (Dileepan et al., 2016; Knowland et al., 2014; Lengfeld et al., 2017), intravenously at P10, P14, and P18 and measured its distribution and levels within the retina (Figure 4A). At P10 and P14, wild-type retinas showed bright puncta of biocytin-TMR within the tissue parenchyma, due to tracer leakage from blood vessels and uptake into neurons (Figures 4B and 4D, white arrows). In contrast, $Apcdd1^{-/-}$ retinas show less biocytin-TMR tracer within the parenchyma compared to wild-type littermate controls at both ages (P10 and P14), which is more pronounced at P14 (Figures 4C and 4E, white arrows). Biocytin-TMR levels within the retina are approximately 30% higher in wild-type compared to $Apcdd1^{-/-}$ at both P10 and P14 (Figure 4H). However, this phenotype is transient, and by P18 both wild-type and $Apcdd1^{-/-}$ retinas show comparable, negligible levels of biocytin-TMR leakage that indicate an almost mature BRB as the superficial plexus matures and ECs acquire barrier properties (Figures 4F–4H). Similar to the retina, the paracellular component of the blood-brain barrier (BBB) in the cerebellum forms prematurely in $Apcdd1^{-/-}$ mice compared to wild-type littermates (Figure S5A, S5B, and S5I). Therefore, while vessel pruning is delayed in *Apcdd1* mutants, paracellular barrier maturation is accelerated, indicating that vessel pruning and acquisition of barrier properties are distinct processes regulated in opposite directions by Apcdd1.

Because paracellular BRB permeability relies on the presence of endothelial cell junctions, we examined expression and subcellular localization of various BRB-forming TJ proteins in wild-type and $Apcdd1^{-/-}$ retinas at P14 and P18. Claudin-5, Occludin, and ZO-1 showed similar localization at cell junctions in endothelial cells of the superficial and deep plexi, in both wild-type and $Apcdd1^{-/-}$ P14 retinas (Figures 4I–4P, white arrows, data not shown). Due to low protein yields from individual mice at these ages, we collected and pooled retinas from entire litters of *Apcdd1*-deficient and wild-type mice. Pooled lysates from an entire litter represent one biological replicate, and we repeated this experiment three times. Western blots show no difference in Cadherin-5 and ZO-1 protein levels between wild-type and $Apcdd1^{-/-}$ retinas (Figures 4Q and 4R). However, $Apcdd1^{-/-}$ retinas display a significant increase in Occludin protein levels at P14 as compared to wild-type tissue (Figures 4Q and 4R). Since Cadherin-5 levels are similar between wild-type and $Apcdd1^{-/-}$ retinas at P14 or P18 (Figures 4Q and 4R), this suggests that the increase in Occludin is not due to a greater number of vessels in $Apcdd1^{-/-}$ P14 retinas. We purified polyA mRNA and quantified the mRNA levels for *Claudin-5*, *Occludin*, and *ZO-1* in P14 wild-type or $Apcdd1^{-/-}$ retinas by qRT-PCR. We found no difference in mRNA levels for any of these transcripts (Figures S5L–S5N), suggesting that Apcdd1 likely regulates Occludin protein stability.

A second defining feature of the barrier is its low rate of transcellular trafficking. ECs within the retina have very few caveolae that express receptors for proteins delivered to the retina parenchyma, including albumin and transferrin (Chow and Gu, 2017; Daneman and Prat, 2015). To measure transcellular permeability, we injected fluorescently labeled albumin intravenously in *Apcdd1*$^{-/-}$ and wild-type littermates (Figure 5A) and measured the amount of albumin associated with blood vessels and retinae in various regions within the superficial vascular plexus, as previously described (Knowland et al., 2014; Lengfeld et al., 2017). We found that *Apcdd1*$^{-/-}$ mice have no significant differences in either endothelium- or parenchyma-associated albumin levels compared to wild-type littermate controls in P10 and P14 retinas (Figures 5B–5K, white arrows). We then examined the levels of Caveolin-1 and PLVAP, proteins that regulate transcytosis, in pooled wild-type and *Apcdd1*$^{-/-}$ retinas at P14 and P18 and found no significant differences between groups (Figures 5L and 5M); this is consistent with no differences in albumin transport across retina ECs in *Apcdd1*$^{-/-}$ mice. Similar results were obtained in the liver and cerebella of wild-type and *Apcdd1*$^{-/-}$ P10 mice (Figures S5C–S5H, S5J, and S5K). Thus, *Apcdd1* is essential for controlling maturation of the paracellular, but not transcellular, barrier properties of retinal and cerebellar endothelium *in vivo*, by likely regulating Occludin protein stability, at least in the retina, and effectively lowering paracellular EC permeability.

Apcdd1-Deficient Brain ECs Display Altered Paracellular and Transcellular Barrier Properties *In Vitro*

Since Apcdd1 is expressed in non-ECs within the retina, we examined whether the changes in barrier properties seen in *Apcdd1*$^{-/-}$ retinas are inherent to the endothelium (Paolinelli et al., 2013). We isolated brain ECs (BECs) from P2 brains of wild-type and *Apcdd1*-deficient pups, using an immunopanning purification method with the endothelial marker CD31 (Daneman et al., 2010a), and cultured them for subsequent *in vitro* experiments. Immunofluorescence for Claudin-5, Occludin, and ZO-1 in confluent monolayers show normal subcellular localization to cell-cell junctions in both wild-type and *Apcdd1*$^{-/-}$ BECs (Figures 6A and 6B, white arrows; data not shown). We measured trans-endothelial electrical resistance (TEER) across BEC monolayers as a readout of EC paracellular barrier integrity and found that *Apcdd1*$^{-/-}$ BECs have increased TEER compared to wild-type BECs, indicating improved paracellular barrier integrity (Figures 6C and 6D). Consistent with these observations, *Apcdd1*$^{-/-}$ BECs create a higher barrier to migration for a small fluorescent dye across the monolayer as compared to wild-type BECs, although this is not statistically significant (Figures S6A, S6C, and S6D). Moreover, addition of XAV-939, a tankyrase inhibitor that blocks Wnt signaling activation (Distler et al., 2013; Lim et al., 2017), to *Apcdd1*$^{-/-}$ BECs reduced TEER similar to that observed in wild-type BECs (Figures S6E and S6F). We examined the ratio of pLRP6/LRP6 and levels of Axin-2 in both wild-type and *Apcdd1*$^{-/-}$ BECs in the absence of Wnt exposure and found that *Apcdd1*$^{-/-}$ BECs have similar levels of Wnt activity (e.g., Axin 2 levels) compared to wild-type BECs (Figures S6H–S6J). However, addition of a low concentration of mouse Wnt3a (250 ng/mL) increased TEER modestly in both wild-type and *Apcdd1*$^{-/-}$ BECs (Figures S6K and S6L), suggesting that higher levels of Occludin and TEER in isolated *Apcdd1*$^{-/-}$ BECs do not depend on continuous Wnt activity. In contrast, there is no difference in transwell migration between wild-type and *Apcdd1*$^{-/-}$ BECs (Figure S6B), consistent with the normal

angiogenic sprouting we observe *in vivo* (Figures 2A–2D and 2M). We then analyzed expression levels of various TJ proteins in BEC lysates by western blotting and found a significant increase in Occludin but not Claudin-5 or ZO-1 protein levels in *Apcdd1*$^{-/-}$ compared to wild-type BECs (Figures 6E and 6F). However, *Occludin* mRNA in ECs was similar in both genotypes (Figure S6G). These data are consistent with our findings *in vivo* from *Apcdd1*$^{-/-}$ retinas (Figures 4Q and 4R). Together, these results suggest that eliminating Apcdd1 in BECs increases both Occludin levels and paracellular barrier resistance, independently of other cells of the neurovascular unit.

We then performed an *in vitro* albumin uptake assay to measure transcellular permeability in BECs (Knowland et al., 2014; Lim et al., 2017; Tiruppathi et al., 2004). Wild-type and *Apcdd1*$^{-/-}$ BECs were incubated for 60 min with albumin-Alexa Fluor 594, and the amount of albumin taken up by BECs was quantified using Fiji software. *Apcdd1*$^{-/-}$ BECs display a significant increase in albumin uptake compared to wild-type BECs, suggesting an increase in endocytosis (Figures 6G–6I). Western blots from BEC lysates revealed increased PLVAP levels in *Apcdd1*-deficient BECs (Figures 6J and 6K); this protein is expressed in the immature embryonic CNS endothelium and associated with fenestrated endothelium and caveolar diaphragms (Hallmann et al., 1995; Stan et al., 1999, 2012). However, addition of low levels of Wnt3a (250 ng/mL) reduced significantly the amount of albumin uptake in *Apcdd1*$^{-/-}$ BECs (Figure S6M). These results indicate that *Apcdd1*$^{-/-}$ BECs exhibit increased transcytosis and a decreased transcellular barrier *in vitro*, which is restored by exposure to Wnt3a. Therefore, continuous exposure to Wnt-3a seems essential to maintain a low transcellular barrier in *Apcdd1*$^{-/-}$ BECs.

Endothelial Apcdd1 Overexpression Promotes Vessel Pruning but Delays Paracellular Barrier Maturation in the Retina

In order to address whether Apcdd1 is sufficient to promote vessel pruning and delay barrier maturation, we generated a gain-of-function (GOF) transgenic mouse line TRE3-mApcdd1-IRES-mCherry (sTg) that overexpresses the full-length mouse Apcdd1 as well as the red fluorescent protein mCherry under the Tet-OFF binary transgenic system. We crossed *Cadherin-5::tTA*$^{+}$ transgenic mice (Sun et al., 2005) with *TRE3-Apcdd1-IRES-mCherry*$^{+}$ to generate doubly transgenic mice (dTg) (Figure 7A). One founder line shows no expression in sTg (*TRE3-Apcdd1-IRES-mCherry*$^{+}$) but strong vascular expression of mCherry in dTg (*Cadherin-5::tTA*$^{+}$; TRE3-Apcdd1-IRES-mCherry^{+}) in P10 retinal blood vessels (Figures 7B–7E). We measured vessel densities in sTg and dTg P10 retinas and found that dTg mice have a reduced vessel density compared to sTg littermates (Figure 7H). We then injected biocytin-TMR intravenously at P14 in sTg and dTg mice, measured its distribution and levels within the retina, and found that dTg mice have higher biocytin-TMR levels compared to sTg mice (Figures 7F, 7G, and 7I). Therefore, endothelial Apcdd1 overexpression produces phenotypes opposite to those of *Apcdd1*$^{-/-}$ mice, suggesting that Apcdd1 tightly regulates vessel pruning and barrier maturation in the developing retina.

DISCUSSION

Precise control of canonical Wnt signaling is necessary for brain angiogenesis, vascular remodeling, and BBB maturation; overexpression or loss of endothelial β-catenin in the brain results in extensive CNS vascular defects and aberrant BBB formation or maintenance (Daneman et al., 2009; Liebner et al., 2008; Stenman et al., 2008; Tran et al., 2016; Zhou et al., 2014). Similarly, loss of endothelial β-catenin signaling in the postnatal retina reduces vessel density, causing premature vessel regression with concomitant loss of BRB function (Phng et al., 2009; Wang et al., 2012; Ye et al., 2009). How canonical Wnt signaling coordinates the timing of these two processes, as its activity progressively decreases in ECs while they transition from an angiogenic to a mature "barrier-forming" state, is poorly understood. Our results showing that loss of the Wnt inhibitor Apcdd1 results in increased transcriptional activity of endothelial β-catenin, leading to delayed vessel pruning but causing premature formation of the BRB in the postnatal retina, whereas endothelial Apcdd1 overexpression produces the opposite phenotype, clarify a crucial step in this process. We discuss below how Apcdd1 sculpts Wnt activity in ECs to coordinate vascular pruning and BRB development, resulting in the mature functional vascular network of the retina.

Apcdd1 is highly expressed in retinal ECs during both angiogenesis and vascular pruning, yet its role is primarily restricted to refining the exuberant immature superficial vascular network. *Apcdd1*-deficient mice show no defects in angiogenic sprouting or development of intra-retinal capillaries in either superficial or deep plexi, but have delayed vascular pruning. This phenotype could be a direct consequence of temporal changes in Norrin signaling within the retina. During retinal development, *Norrin* remains relatively constant (P1–P17), while *Fz4* fluctuates with peak expression at P17. Conversely, *Lrp5/6* levels are highest at P1 then steadily decrease by P7, persisting into adulthood (Chen et al., 2012). The reduction in Lrp5/6 levels and presumably Fz4/Lrp5/6 activity at P7 corresponds to the end of angiogenic growth within the superficial plexus, EC sprouting into the outer plexiform layer and the onset of vessel pruning (Stahl et al., 2010). We propose that during vessel pruning, ECs with intermediate levels of β-catenin activity undergo regression, while those retaining high levels of β-catenin activity fail to regress (Figure 7J). Apcdd1 functions at this stage to inhibit Norrin/Fz4/Lrp5/6 signaling in the subset of retinal ECs that will undergo regression and pruning (Figure 7J). Consistent with this model, loss of *Apcdd1* results in sustained high levels of β-catenin activity in ECs (Figures S2G–S2O) that block, albeit transiently, the transition from angiogenesis to vascular remodeling. The hypervascularized phenotype in *Apcdd1*$^{-/-}$ retinas is opposite to that seen in *Ndp*, *Fz4*, and *Lrp5/6* mutants or *Apcdd1* GOF mice, which display reduced vessel densities in the superficial plexus (Chen et al., 2012; Luhmann et al., 2005; Xia et al., 2010; Xu et al., 2004). Norrin overexpression upregulates several transcriptional targets including Timp3, a matrix metalloproteinase (MMP) inhibitor, pro-collagens, and pro-collagen processing enzymes that attenuate vascular remodeling by preventing vessel regression (Zhu et al., 2000). It is likely that Apcdd1 reduces Norrin signaling to upregulate transcriptional Wnt targets that are necessary for matrix remodeling during vessel regression.

While *Apcdd1* mutants show delayed vascular remodeling, acquisition of some endothelial barrier properties is accelerated. At ages P10 and P14, *Apcdd1*$^{-/-}$ retinas show decreased

uptake of the biocytin-TMR tracer, indicating that their junctional integrity and paracellular barriers are more mature. Consistent with our *in vivo* results, *Apcdd1*$^{-/-}$ BECs have increased TEER as compared to wild-type BECs, indicating that *Apcdd1* functions cell autonomously in ECs to promote formation of the mature paracellular barrier. Conversely, *Apcdd1* GOF mice show delayed paracellular barrier maturation. A potential explanation for how Apcdd1 inhibits formation of the paracellular barrier could be controlling Occludin protein but not mRNA levels, because Occludin protein levels are higher in *Apcdd1*$^{-/-}$ retinas and BECs. While Claudin-3 and -5 are known downstream targets of canonical Wnt signaling in CNS ECs (Chen et al., 2012; Liebner et al., 2008), Occludin is also reduced in cerebellar ECs from *Norrin*-deficient mice (Wang et al., 2012). Conversely, intra-cerebroventricular injection of recombinant Norrin following subarachnoid hemorrhage-induced BBB breakdown increases Occludin expression and reduces BBB leakage (Chen et al., 2015). These loss- and gain-of-function studies are consistent with Occludin being a Norrin/Fz4/Lrp5 target gene. Additionally, downregulation of Occludin expression correlates with barrier breakdown during both experimentally induced diabetes (Antonetti et al., 1998) and neutrophil-induced BBB rupture (Bolton et al., 1998), suggesting that eliminating Occludin is crucial to increase paracellular barrier permeability. Occludin belongs to the family of tight junction-associated MARVEL proteins (TAMP) that include Occludin, Tricellulin, and MarvelD3. These proteins are essential for proper regulation and positioning of tight junction proteins to cell-cell junctions. Higher levels of Occludin could promote precocious localization of other tight junction-associated proteins to cell-cell junctions, or alter intracellular trafficking of tight junction proteins in *Apcdd1*$^{-/-}$ as compared to wild-type ECs, as has been observed for epithelial cells (Haseloff et al., 2015). Based on Apcdd1 loss- and gain-of-function phenotypes, we hypothesize that Apcdd1 lowers β-catenin activity to both reduce Occludin levels and delay tight junction maturation at the BRB (Figure 7J).

While loss of Apcdd1 accelerates TJ maturation, it has no significant effect on transcellular permeability *in vivo*. *Apcdd1* mutant mice show no differences in either albumin uptake or Caveolin-1 and PLVAP protein levels in the retina compared to wild-type litter-mates. However, *in vitro* purified *Apcdd1*$^{-/-}$ BECs show a marked increase in albumin uptake accompanied by increased PLVAP protein. How can these findings be reconciled? In ECs, albumin is trafficked through caveolae, a subdomain of cholesterol-rich glycolipid rafts that require the GTPase activity of dynamin for membrane budding (Minshall et al., 2000). PLVAP is an integral membrane protein that localizes to fenestrae and caveolar stomatal diaphragms (Stan et al., 2012) and is expressed transiently in immature CNS ECs until E16.5; its downregulation is necessary for a mature BBB (Hallmann et al., 1995; Zhao et al., 2015). EC-pericyte interactions are critical to downregulate PLVAP expression, because *Pdgfr*β$^{-/-}$ mice that lack pericytes show increased endothelial PLVAP expression and increased uptake of Evans blue dye in the brain (Daneman et al., 2010b). Therefore, we hypothesize that lack of Apcdd1 in BECs promotes maintenance of PLVAP-expressing fenestrae, allowing for increased albumin uptake *in vitro*. This defect is likely inhibited *in vivo* due to pericyte-derived signals that effectively lower PLVAP expression in *Apcdd1*$^{-/-}$ retinal ECs, because pericyte coverage is normal in *Apcdd1*$^{-/-}$ retinas. Alternatively continuous Wnt activity may be required to maintain low transcellular permeability of *Apcdd1*$^{-/-}$ BECs since addition of Wnt3a reduces the transcellular defect in isolated mutant

BECs (Figure S6M). It was recently suggested that BRB maturation occurs primarily via a gradual suppression of transcytosis, whereas the paracellular component of the barrier forms very early (P3) in retina development (Chow and Gu, 2017). Our findings do not support this model of BRB maturation, because we find that the paracellular component of the BRB does not mature until P18 and *Apcdd1*$^{-/-}$ mice display premature maturation of the paracellular, but not transcellular, BRB compared to wild-type littermates.

Taken together, our loss- and gain-of-function data reveal a crucial role for Apcdd1 in regulating discrete levels of β-catenin transcriptional activity that are mediated by Norrin/Fz4/Lrp5/6 signaling in retinal ECs and are essential for vessel pruning and forming a functional barrier. On the one hand, Apcdd1 decreases endothelial β-catenin activity to induce a transcriptional program that promotes EC regression during vessel pruning, while on the other hand the presence of Apcdd1 ensures that endothelial cells with intermediate β-catenin activity, which are destined for regression, do not form a functional barrier (Figure 7J). By this means, Apcdd1 tightly coordinates the cessation of vascular pruning with BRB maturation to ensure that maturation does not occur prematurely in vessels that will be eliminated. Although the role of Apcdd1 as an inhibitor of Norrin/Fz4/Lrp5/6 signaling is transient, it serves to finely tune the levels of β-catenin appropriate for the various stages of angiogenesis and barrier development. Future investigations will allow us to clarify the molecular mechanisms through which these diverse effects are mediated.

STAR★METHODS

KEY RESOURCES TABLE

REAGENT or RESOURCE	SOURCE	IDENTIFIER
Antibodies		
Mouse monoclonal anti-β-actin (clone AC-15)	Abcam	Cat #ab6276, Lot #GR185659-3, RRID: AB_2223210
Mouse monoclonal anti-β-actin (clone AC-15)	Novus Biologicals	Cat #NB600-501, Lot #64M4789V, RRID: AB_10077656
Mouse monoclonal anti-Claudin-5 (clone 4C2C2)	ThermoFisher	Cat #352500, Lot #1456673A, RRID: AB_87321
Rabbit polyclonal anti-Claudin-5	ThermoFisher	Cat #34-1600, Lot #QG215200, RRID: AB_86930
Rabbit polyclonal anti-ZO-1	ThermoFisher	Cat #617300, Lot #12484048, RRID: AB_138452
Mouse monoclonal anti-ZO-1 (clone ZO1-1A12)	ThermoFisher	Cat #33-9100, RRID: AB_87181
Rabbit polyclonal anti-Occludin	ThermoFisher	Cat #711500, Lot #944954A, RRID: AB_88065
Rabbit polyclonal anti-Caveolin-1	Abcam	Cat #ab18199, Lot #GR13846-1, RRID: AB_444314
Rabbit polyclonal anti-SDRP (Cavin 2)	Abcam	Cat #ab113876, Lot #GR134553-1, GR125784-3, GR125784-7, RRID: AB_10860033
Rabbit polyclonal anti-PLVAP	proteintech	Cat #14452-1-AP, Lot #00005529, RRID: AB_2166100
Rabbit polyclonal anti-Collagen IV	Abcam	Cat #ab6586, Lot #GR248055-2, RRID: AB_305584

REAGENT or RESOURCE	SOURCE	IDENTIFIER
Rhodamine-labeled *Griffonia* (*Bandeiraea*) *Simplicifolia* lectin I (GSL I, BSL I)	Vector Laboratories	Cat#RL-1102, RRID: AB_2336492
Fluorescein-labeled *Griffonia* (*Bandeiraea*) *Simplicifolia* lectin I (GSL I, BSL I)	Vector Laboratories	Cat #FL-1101, RRID: AB_2336490
Guinea pig anti mouse Islet-1	Gift from Thomas M. Jessell. The antibody was published in the following publication: Shimomura et al., 2010	N/A
Rabbit polyclonal anti-rhodopsin	Abcam	Cat #ab3424, Lot #GR193394-5, RRID: AB_2269503
Rabbit polyclonal anti-neurofilament	Biolegend	Cat #801703, Lot#D14FF01278
Rabbit polyclonal anti-VE-Cadherin	Abcam	Cat # ab33168, Lot # GR192430-1, RRID: AB_870662
Rabbit polyclonal anti-Sox9	Millipore	Cat #ABE571, Lot #2535307
Goat polyclonal anti-Sox17	R&D Systems	Cat #AF1924, RRID: AB_355060
Rabbit polyclonal anti-cleaved caspase 3	Cell Signaling	Cat #9664S, Lot#20, RRID: AB_10694088
Rabbit polyclonal anti-NG2	Millipore	Cat #AB5320, Lot #2834672, RRID: AB_91789
Rabbit polyclonal anti-phosphoLRP6	Cell Signaling	Cat #2568S, Lot #5, RRID: AB_2139327
Rabbit polyclonal anti-LRP6	Cell Signaling	Cat # 3395S, Lot #3, RRID: AB_1950408
Rabbit polyclonal anti-active β-catenin	Cell Signaling	Cat #8814S, Lot #3, RRID: AB_11127203
Rabbit polyclonal anti-β-catenin	Abcam	Cat #ab3572, Lot #GR184212-36, RRID: AB_725966
Rabbit polyclonal anti Axin-2	Abcam	Cat # ab32197, Lot #GR2T1869-1, RRID: AB_2290204
Goat polyclonal anti-mouse IgG IRDye 680	LICOR	N/A
IRDye 800	LICOR	N/A
Chemicals, Peptides, and Recombinant Proteins		
Biocytin-TMR (5-(and-6)-tetramethylrhodamine biocytin)	ThermoFisher	Cat #T12921
Bovine Serum Albumin (BSA), AlexaFluor 488 conjugate	ThermoFisher	Cat #A13100
Bovine Serum Albumin (BSA), AlexaFluor 594 conjugate	ThermoFisher	Cat #A13101
Mouse Collagen IV	Corning	Cat #354233
XAV939	Sigma	Cat #X3004
Recombinant Mouse Wnt-3a protein	R&D Systems	Cat # 1324-WN-002
EdU	ThermoFisher	Cat #A10044, Lot #1482215
Critical Commercial Assays		
Click-iT AlexaFluor 594 Imaging Kit	ThermoFisher	Cat #C10245 Lot #1646258
Experimental Models: Cell Lines		

REAGENT or RESOURCE	SOURCE	IDENTIFIER
Mouse: Primary Brain Microvascular Endothelial Cells	Cell Biologics	Cat #C57-6023, Lot#070613T2MP, 011513
Mouse: custom-isolated *Apcdd1*$^{-/-}$ Brain Microvascular Endothelial Cells	Cell Biologics	Cat #Custom Isolation, Lot #C0041514, 101714
Experimental Models: Organisms/Strains		
Mouse: CD-1 mouse strain	Charles River	Strain Code # 022
Mouse: *Apcdd1*$^{-/-}$ strain (CD-1 background).	This publication	N/A
Mouse: TRE3-Apcdd1-IRES-mCherry transgenic strain	This publication	N/A
Cadherin-5::tTA$^{+/-}$	Jackson Laboratories	Strain Code # 013585
Oligonucleotides		
GAPDH F 5′-AAC TTT GGC ATT GTG GAA GG-3′	IDT	N/A
GAPDH R 5′-ACA CAT TGG GGG TAG GAA CA-3′	IDT	N/A
Claudin-5 F 5′-TTT AGC CAT GGG GTC TGC AG-3′	IDT	N/A
Claudin-5 R 5′-CAC GAT GTT GTG GTC CAG GA-3′	IDT	N/A
ZO-1 F 5′-TGA ACG TCC CTG ACC TTT CG-3′	IDT	N/A
ZO-1 R 5′-GCT CTG AAC GTT GGT CAG GA-3′	IDT	N/A
Occludin F 5′-TTT CCT GCG GTG ACT TCT CC-3′	IDT	N/A
Occludin R 5′-AAA ACA GTG GTG GGG AAC GT-3′	IDT	N/A
TRE3Gfor 5′-CAC GAG GCC TTT CGT CTT CAA GAA TTC CTC GAG-3′	IDT	N/A
SVpArev 5′-AAG ATA CAT TGA TGA GTT TGG ACA AAC CAC-3′	IDT	N/A
Apcdd1 WT F 5′-GAG TGT CCC CGA CTC CGA CTC T-3′	IDT	N/A
Apcdd1 WT R 5′-ATG TGT TGA GTT ATT CCC GGA AG-3′	IDT	N/A
Apcdd1 mut F 5′-GCC CAT CTG GGA TAG TAC ATG TG-3′	IDT	N/A
Apcdd1 mut R 5′-CCT GGA CTG AGG GCC ATA GGT AAG AGG-3′	IDT	N/A
Recombinant DNA		
pTRE3G-IRES vector	Clontech	N/A
pCR4-TOPO vector	ThermoFisher	N/A

CONTACT FOR REAGENT AND RESOURCE SHARING

Further information and requests for resources and reagents should be directed to the Lead Contact, Dr. Dritan Agalliu (da191@cumc.columbia.edu).

EXPERIMENTAL MODEL AND SUBJECT DETAILS

Cell Lines and Cell Culture—Primary mouse BECs were either isolated by CD31^{+} immunopanning from P2 wild-type and *Apcdd1*$^{-/-}$ pups, as described (Daneman et al., 2010a) or purchased from Cell Biologics. Both male and female wild-type or *Apcdd1*$^{-/-}$ mice were used to isolate primary BECs from the brain. Cell were were plated on Collagen IV-coated plates and cultured in endothelial cell media supplemented with growth factors

and 5% FBS (Cell Biologics) to promote formation of confluent monolayers. Cells were switched to media with low serum (1% FBS) in the absence of growth factors after reaching confluence and prior to starting experimental treatments.

Animals—All experimental procedures were approved by the IACUC regulatory bodies at Columbia University Medical Center and the University of California at Irvine.

Generation of *Apcdd1* mutant mice and genotyping—We employed a previously described *Apcdd1* mutant strain in which loxP sites had been engineered to flank exons 2 and 3 (Figure S1) (Turakainen et al., 2009). We crossed *Apcdd1*Ex2,3$^{flox/flox}$ mice to a strain bearing the Cre recombinase under a heat shock promoter, which is ubiquitously expressed (Dietrich et al., 2000), to yield *Apcdd1*Δex2,3$^{-/-}$ mutants (Figure S2A). *Apcdd1*Δex2,3$^{-/-}$ (hereafter designated *Apcdd1*$^{-/-}$) mutants are viable and fertile and do not exhibit any overt embryonic developmental defects. PCR primers for the *Apcdd1* wild-type allele are forward (5′-GAGTGTCCCCGACTCCGACTCT) and reverse (5′-ATGTGTTGAGTTATTCCCGGAAG). PCR primers for the *Apcdd1* mutant allele are forward (5′-GCCCATCTGGGATAGTACATGTG) and reverse (5′-CCTGGACT GAGGGCCATAGGTAAGAGG). Amplification was performed using *Taq* DNA polymerase with standard *Taq* buffer (New England Biolabs). PCR thermal cycler was programmed for 3 min at 94°C for initial denaturation, followed by 30 cycles of 30 s at 94°C for denaturation, 30 s at 60°C for annealing, 90 s at 72°C for extension and 10 min at 72°C for final extension. The fragment sizes for Apcdd1 wild-type and mutant alleles are 1 kb and 1.8 kb, respectively (Figure S2B). Both male and female wild-type or *Apcdd1*$^{-/-}$ mice were used for experiments.

Generation of a *TRE3-Apcdd1-IRES-mCherry*+ transgenic strain—First, a 0.7 kb SmaI/XbaI fragment containing the coding sequence for the red fluorophore mCherry was cloned into EcoRV/NheI sites within the second multiple cloning site of the pTRE3G-IRES vector (Clontech). This placed the mCherry start codon 41 nucleotides downstream of the preferential start codon after the IRES sequence, and therefore out of frame; however, translation of mCherry from this bicistronic mRNA was confirmed by tetracycline-induced transfection in HEK293 cells before constructs were injected. Next, the full-length mApcdd1 ORF (1.5 kb) was amplified using Q5 High-Fidelity DNA polymerase (New England Biolabs) with SalI (5′) and ClaI (3′) sites in the amplifying primers. This was cloned into the SalI/ClaI sites within the first multiple cloning site of pTRE3G-IRES-mCherry to yield the complete transgene construct. The Apcdd1 sequence amplified by PCR was confirmed to be error-free by sequencing before DNA injection.

For injection into fertilized oocytes, the complete pTRE3G-Apcdd1-IRES-mCherry-SV40polyA gene (~4.3 kb) was amplified from pTRE3G using the primers TRE3Gfor (5′-CACGAGGCCCTTTCGTCTTCAAGAATTCCTCGAG) and SVpArev (5′-AAGATACATTGATGAGTTTGGACAAACCAC) and subcloned into the pCR4-TOPO vector (Life Technologies). Clones were doubly digested with EcoRI (to release the transgene) plus SphI (to cut pCR4-TOPO into two smaller pieces) and provided to the Transgenic Mouse Facility at the University of California, Irvine. Transgenic founder animals were recovered at expected frequencies (16/103 = 16% for Apcdd1), mated

individually to establish independent lines, then screened by crossing to the *Cadherin-5::tTA*$^{+}$ (Sun et al., 2005) driver strain to assay Tet-dependent expression of mCherry in the vascular endothelium. Both male and female sTg or dTg mice were used for experiments.

METHODS DETAILS

RNA *in situ* hybridization and fluorescent western blotting—Both alkaline phosphatase and double fluorescent *in situ* hybridization were performed as described (Lengfeld et al., 2017) using anti-sense mRNA probes for full-length mouse *Apcdd1*, *Apcdd1* (exons 2–3), *Claudin-5, PDGFR*β, *Sox9* and *Norrin*. Fluorescent *in situ* hybridization for *Apcdd1* was followed by immunostaining for Caveolin-1. Fluorescent western blot analysis and quantitation were performed as described (Knowland et al., 2014). See Key Resources Table for specific details about the antibodies.

Tissue isolation—Retinas, cerebella and livers were harvested from wild-type and *Apcdd1*$^{-/-}$ mice. Mice were perfused with phosphate-buffered saline (PBS) and 4% paraformaldehyde (PFA), tissue was fixed for 4 h with cold 4% PFA and washed with PBS. Whole-mount retinas were dissected to isolate the retinal cup and relieving cuts were made prior to staining. Retinas and livers collected for sectioning were cryoprotected with 30% sucrose in PBS and embedded in OCT (TissueTek, Sakura-Finetek).

Immunofluorescence—Whole-mount retinas were stained with the following primary antibodies: BSL-FITC (1:500, Vector Laboratories), BSL-rhodamine (1:750, Vector Laboratories), anti-Collagen IV (1:2000, Abcam), anti-cleaved Caspase 3 (1:500, Cell Signaling) and anti-NG2 (1:500, Millipore). Imaging of whole-mount retinas was performed with a Zeiss LSM700 confocal microscope. Sectioned retinas were stained with the following primary antibodies: anti-Caveolin-1 (1:2000, Abcam), anti-Sox17 (1:50, R&D Systems), anti-Islet-1 (1:5000), anti-Sox9 (1:1000, Millipore), anti-Neurofilament (1:1000, Abcam) and anti-Rhodopsin (1:500, Abcam). Sectioned retinas were imaged with a Zeiss Axioimager.

Western blotting—Retinas, brains and livers were collected from mice after perfusion with PBS. Collected tissue was homogenized in lysis buffer containing protease and phosphatase inhibitors using a Dounce homogenizer followed by sonication. Protein levels in P10, P14 and P18 retinas were measured by fluorescent western blot analysis and quantitation was performed using the LICOR (LICOR, Lincoln, NE) system, as described (Knowland et al., 2014). Western blot analysis used the following primary antibodies: anti-ZO-1 (1:1000, ThermoFisher Scientific), anti-Occludin (1:250, ThermoFisher), anti-Caveolin-1 (1:1000, Abcam), anti-PLVAP (1:500, ProteinTech), anti-Cadherin-5 (1:500, Abcam), anti-pLRP6 (1:500, Cell Signaling), anti-LRP6 (1:500, Cell Signaling), anti-active β-catenin (1:500, Cell Signaling), anti-β-catenin (1:500, Abcam), anti-β-actin (1:10000, Abcam) and anti-Axin2 (1:1000, Abcam). IRDyes 680 and 800 (1:10000; LI-COR) were used as secondary antibodies. Fluorescent quantification of protein levels was done using the Odyssey SA infrared imaging system. Values are displayed as protein levels corrected with β-actin and normalized to wild-type control values.

Primary mouse BECs were grown on poly-D-lysine- and collagen IV-coated plates to ~90% confluence in 10% FBS media, then switched to 1% FBS media for 48 hr. Cells were then harvested and lysed in RIPA buffer with protease and phosphatase inhibitors. Western blot analysis used the following primary antibodies: anti-Claudin-5 (1:2000, ThermoFisher Scientific), anti-Occludin (1:1000, ThermoFisher Scientific), anti-ZO-1 (1:1000, ThermoFisher Scientific), anti-Caveolin-1 (1:4000, Abcam), anti-Cavin 2 (1:1000, Abcam), anti-PLVAP (1:500, ProteinTech) and anti-β-actin (1:10,000, Abcam) anti-pLRP6 (1:500, Cell Signaling), anti-LRP6 (1:500, Cell Signaling), and anti-Axin2 (1:1000, Abcam). IRdyes 680 and 800 (1:20000, LI-COR) were used as secondary antibodies. Fluorescent quantification of protein levels was done using the Odyssey SA infrared imaging system. Values are displayed as protein levels corrected with β-actin and normalized to wild-type control values. Experiments were repeated five times.

Vessel density, vessel sprout number and vein diameter analysis—Vessel densities for whole-mount P5–P14 retinas were measured using intersection analysis in Fiji. A 2500–5000 μm^2 grid was placed randomly over the retinal leaflet. Each intersection point of the grid served as a test point. Test points overlaying the entire leaflet vasculature from the optic nerve to the angiogenic front were counted as positive “crossing” points. Test points that did not overlay the vasculature were negative “non-crossing” points. The fractional vascular density per animal was calculated by dividing the number of crossing points by the total number of test points overlaying retina leaflets. Vessel sprout analysis was performed by counting the number of EC sprouts at the vascular front of imaged P5 whole-mount retinas in Fiji. Vein diameters of P8–P14 imaged whole-mount retinas were measured in Fiji. The diameter of each vein was measured at three different locations and the values averaged.

EdU incorporation—*Apcdd1*$^{-/-}$ and wild-type littermate control animals were injected intravenously (i.v.) with 1 μL of 10 mg/mL EdU per gram body weight. After 4 hr, retinas were collected and fixed. EdU detection was performed using the Click-iT AlexaFluor 594 Imaging kit (Thermofisher Scientific). Retinas were stained with BSL-FITC (Vector Laboratories) and the superficial plexus imaged with confocal microscopy. EdU^+ cells that co-localize with retina vessels were counted using Fiji, and numbers of EdU^+ cells were normalized to the vessel area or vessel length. To calculate vessel area, the area of each analyzed leaflet was traced and measured in Fiji. The percent vessel density of each leaflet was multipled by the total area of each leaflet to generate the vessel area for each leaflet. The sum of EdU^+ cells for all leaflets analyzed was normalized to the sum of analyzed vessel area for each animal.

Analysis of ECM sleeves—P10–P14 retinas from *Apcdd1*$^{-/-}$ and wild-type mice were isolated and stained with BSL-rhodamine (Vector Laboratories) and Collagen IV (Abcam). ECM analysis was performed by counting empty ECM sleeves that were Collagen IV^+ and BSL-rhodamine. The number of empty ECM sleeves was normalized to the vessel area as described above.

***In vivo* biocytin-TMR assay—**Mice were injected i.v. with a 1% biocytin-TMR solution (Thermofisher Scientific) and perfused after 30 min. Retinas, cerebella and livers were collected, and whole-mount retinas or cerebella and liver sections were stained with BSL-FITC. Multiple areas of whole-mount retinas (superficial plexus) and cerebella or livers were imaged with a Zeiss LSM700 confocal microscope and analyzed using Fiji software. The intensity of biocytin-TMR outside of the vessels (tracer leakage) was measured by line scan analysis as described (Dileepan et al., 2016; Knowland et al., 2014). Biocytin-TMR signal intensities in the retina and cerebella were normalized to those of livers.

***In vivo* albumin uptake assay—**Mice received i.v. injections of 1% albumin-AlexaFluor 488 (Life Technologies). After 60 min, mice were perfused. Collected retinas and cerebella were stained with BSL-rhodamine (retina) or Glut-1 (cerebella). Multiple areas of whole-mount retinas in the superficial plexus, cerebella, and livers were imaged with a Zeiss LSM700 confocal microscope and analyzed using Fiji software. Endothelium-and parenchyma-associated albumin levels were measured as described (Knowland et al., 2014). The area of albumin present in the retina was normalized to that of the liver for each animal.

Trans-endothelial electrical resistance measurement—Primary mouse BECs were purified from wild-type and *Apcdd1*$^{-/-}$ brains as described (Daneman et al., 2010a), plated on poly-D-lysine- and Collagen IV-coated gold electroarray 96-well plates (Applied Biophysics), and grown in endothelial cell media supplemented with growth factors and 10% FBS media (Cell Biologics) to maximum resistance. Cells were switched to 1% FBS and the resistance recorded every 30 min for 48 hr using the ECIS Z-θ system (Applied Biophysics). In some experiments either Wnt3a (250 ng/mL) or 5 μM XAV-939, a tankyrase inhibitor that blocks Wnt signaling activation (Distler et al., 2013; Lim et al., 2017), were added to a subset of wild-type or *Apcdd1*$^{-/-}$ BECs when cells were switched to media with low 1% FBS, and the resistance recorded every 30 min for 48 hr using the ECIS Z-θ system (Applied Biophysics). Resistance curves were generated using GraphPad Prism software. Areas under the curve were quantified for the final 48 hr after cells reached maximum resistance using GraphPad Prism software.

***In vitro* albumin uptake assay—**Primary mouse BECs from wild-type and *Apcdd1*$^{-/-}$ animals were grown on poly-D-lysine- and Collagen IV-coated glass coverslips to ~90% confluence in 10% FBS media, then switched to 1% FBS media for 48 hr. In some experiments wild-type and *Apcdd1*$^{-/-}$ BECs were incubated with mouse Wnt3a (250 ng/mL) for 48 hr. Cells were incubated with 50 μg/mL albumin conjugated to AlexaFluor 594 (ThermoFisher Scientific) for 60 min at 37°C and excess albumin was washed away with PBS. BECs were fixed with 4% para-formaldehyde and mounted in Vectashield containing DAPI (Vector Laboratories). BECs were imaged using a Zeiss LSM 700 confocal microscope. Albumin quantification was accomplished by measuring the area of albumin and dividing by the number of cells in the field using Fiji software.

Sox17 and retinal population analysis—Multiple areas of sagittally sectioned P10 retinas were imaged with a Zeiss Axioimager and quantification performed in Fiji. Sox17 signal intensity was measured by line scan analysis in nuclei (DAPI^{+}; Sox17^{+}) of

Caveolin-1$^+$ endothelial cells of the superficial plexus. Line scan analysis was done in nuclei for 130–200 ECs per animal. Isl-1$^+$ cells in the GCL or INL and Sox9$^+$ cells in the INL were counted in Fiji (7–8 sagittal retina sections per animal for Isl-1; 3–13 images per animal for Sox9). The layer width of neurofilament and rhodopsin was measured in Fiji (7–8 sagittal retina sections per animal). The width was measured at eight different locations from each section and the values averaged.

Cleaved Caspase 3 analysis—Whole-mount P10 retinas were stained with BSL-FITC and anti-cleaved Caspase 3. Multiple areas of the distal or mid-leaflet vascu-lature were imaged at 40× with a Zeiss LSM700 confocal microscope. The number of cleaved Caspase 3$^+$ ECs were counted in each image. The vessel area of each analyzed image was measured by signal thresholding in Fiji. The number of cleaved Caspase 3$^+$ ECs was normalized to vessel area for each image. 9–16 images of the distal vasculature and 8–14 images of the mid-leaflet vasculature per animal were analyzed.

qRT-PCR analysis for mRNA levels of tight junction proteins—PolyA mRNA was purified from either wild-type or *Apcdd1*$^{-/-}$ P14 retinas (3 mice/genotype) or wild-type and *Apcdd1*$^{-/-}$ confluent 10 cm dishes of BECs (3 individual experiments) using the RNAeasy Micro kit (QIAGEN). qRT-PCR was performed for *Claudin-5*, *Occludin*, *ZO-1*, and *GAPDH* mRNAs using the primers described in Key Resources Table and the following PCR conditions: 95°C for 30 s, followed by 39 cycles of 95°C for 10 s, 60°C for 1 min and 65°C for 30 s.

***In vitro* tracer leakage assay—**Primary mouse BECs were isolated by CD31$^+$ immunopanning from P2 wild-type and *Apcdd1*$^{-/-}$ pups, as described (Daneman et al., 2010a), and were plated on Collagen IV-coated 3.0 μm pore size transwell inserts at 50,000 cells/1.1cm^2. Cells were grown in 10% FBS media for 48 hr then switched to 1% FBS media for 24 hr. IRDye 800CW carboxylate (LICOR) tracer was added to the top chamber in a buffer containing HBSS, 4.2 mM $NaHCO_3$, 10 mM HEPES and 1 mg/mL bovine serum albumin. The tracer was allowed to diffuse to the bottom chamber for 10 min. 100 μL aliquots were collected in a 96-well round-bottom plate after 5 and 10 min. Fluorescence was measured using the Odyssey SA infrared imaging system.

Transwell migration assay—Primary mouse wild-type and *Apcdd1*$^{-/-}$ BECs were plated on fibronectin-coated 3.0 μm pore size transwell inserts at 100,000 cells/1.1cm^2. Cells were grown in 10% FBS media and switched to 0.1% FBS media 4 hr prior to plating on transwell inserts. 24 hr after plating, cells were fixed with 4% PFA. Cells that had migrated to the underside of the transwell insert were stained with DAPI and counted.

QUANTIFICATION AND STATISTICAL ANALYSIS

ImageJ software was utilized for the quantitation of immunofluorescence images. Statistical analysis was performed using GraphPad Prism software version 7.0. Unpaired t test was used to compare the differences between two groups in studies. Two-way ANOVA followed by Tukey's post hoc test was performed to compare the differences among groups in the cell culture studies. Differences between groups were presented as the mean ± SEM or SD as

noted in the figure legends. The sample size (n) for each experiment is indicated in the figure legends and results section. All tests were two sided and p values < 0.05 were considered to be statistically significant.

Supplementary Material

Refer to Web version on PubMed Central for supplementary material.

Acknowledgments

We thank Eva Morozko and Marc Abboud for assistance with some experiments, Sarah E. Lutz for advice on quantitative analysis of vascular density in the retina, Juha Partanen at the University of Helsinki for providing *Apcdd1* floxed embryos, and Thong Ma and Un Kang at Columbia University Medical Center for help with the qRT-PCR experiments. J.M., T.C., J.S., S.S., and D.A. are supported by grants from the NIH (#R01-HL116995, #R56-MH109987, #R01MH112849), the American Heart Association (#12BGOA11560014), and the Leducq Foundation. D.A. is partially supported by an unrestricted gift from John. F. Castle to the Stroke Division in the Department of Neurology at Columbia University Medical Center. B.C. was supported by an Undergraduate Research Opportunity (UROP) Fellowship.

References

Adams RH, Alitalo K. Molecular regulation of angiogenesis and lymphangiogenesis. Nat Rev Mol Cell Biol. 2007; 8:464–478. [PubMed: 17522591]

Antonetti DA, Barber AJ, Khin S, Lieth E, Tarbell JM, Gardner TW, Penn State Retina Research Group. Vascular permeability in experimental diabetes is associated with reduced endothelial occludin content: vascular endothelial growth factor decreases occludin in retinal endothe-lial cells. Diabetes. 1998; 47:1953–1959. [PubMed: 9836530]

Bilic J, Huang YL, Davidson G, Zimmermann T, Cruciat CM, Bienz M, Niehrs C. Wnt induces LRP6 signalosomes and promotes dishevelled-dependent LRP6 phosphorylation. Science. 2007; 316:1619–1622. [PubMed: 17569865]

Bolton SJ, Anthony DC, Perry VH. Loss of the tight junction proteins occludin and zonula occludens-1 from cerebral vascular endothelium during neutrophil-induced blood-brain barrier breakdown in vivo. Neuroscience. 1998; 86:1245–1257. [PubMed: 9697130]

Chen J, Stahl A, Krah NM, Seaward MR, Joyal JS, Juan AM, Hatton CJ, Aderman CM, Dennison RJ, Willett KL, et al. Retinal expression of Wnt-pathway mediated genes in low-density lipoprotein receptor-related protein 5 (Lrp5) knockout mice. PLoS ONE. 2012; 7:e30203. [PubMed: 22272305]

Chen Y, Zhang Y, Tang J, Liu F, Hu Q, Luo C, Tang J, Feng H, Zhang JH. Norrin protected blood-brain barrier via frizzled-4/β-catenin pathway after subarachnoid hemorrhage in rats. Stroke. 2015; 46:529–536. [PubMed: 25550365]

Cho C, Smallwood PM, Nathans J. Reck and Gpr124 are essential receptor cofactors for Wnt7a/Wnt7b-specific signaling in mammalian CNS angiogenesis and blood-brain barrier regulation. Neuron. 2017; 95:1221–1225.

Chow BW, Gu C. The molecular constituents of the blood-brain barrier. Trends Neurosci. 2015; 38:598–608. [PubMed: 26442694]

Chow BW, Gu C. Gradual suppression of transcytosis governs functional blood-retinal barrier formation. Neuron. 2017; 93:1325–1333.e3. [PubMed: 28334606]

Corada M, Orsenigo F, Morini MF, Pitulescu ME, Bhat G, Nyqvist D, Breviario F, Conti V, Briot A, Iruela-Arispe ML, et al. Sox17 is indispensable for acquisition and maintenance of arterial identity. Nat Commun. 2013; 4:2609. [PubMed: 24153254]

Daneman R, Prat A. The blood-brain barrier. Cold Spring Harb Perspect Biol. 2015; 7:a020412. [PubMed: 25561720]

Daneman R, Agalliu D, Zhou L, Kuhnert F, Kuo CJ, Barres BA. Wnt/beta-catenin signaling is required for CNS, but not non-CNS, angiogenesis. Proc Natl Acad Sci USA. 2009; 106:641–646. [PubMed: 19129494]

Daneman R, Zhou L, Agalliu D, Cahoy JD, Kaushal A, Barres BA. The mouse blood-brain barrier transcriptome: a new resource for understanding the development and function of brain endothelial cells. PLoS ONE. 2010a; 5:e13741. [PubMed: 21060791]

Daneman R, Zhou L, Kebede AA, Barres BA. Pericytes are required for blood-brain barrier integrity during embryogenesis. Nature. 2010b; 468:562–566. [PubMed: 20944625]

Dejana E. The role of wnt signaling in physiological and pathological angiogenesis. Circ Res. 2010; 107:943–952. [PubMed: 20947863]

Dietrich P, Dragatsis I, Xuan S, Zeitlin S, Efstratiadis A. Conditional mutagenesis in mice with heat shock promoter-driven cre transgenes. Mamm Genome. 2000; 11:196–205. [PubMed: 10723724]

Dileepan T, Smith ED, Knowland D, Hsu M, Platt M, Bittner-Eddy P, Cohen B, Southern P, Latimer E, Harley E, et al. Group A Streptococcus intranasal infection promotes CNS infiltration by streptococcal-specific Th17 cells. J Clin Invest. 2016; 126:303–317. [PubMed: 26657857]

Distler A, Deloch L, Huang J, Dees C, Lin NY, Palumbo-Zerr K, Beyer C, Weidemann A, Distler O, Schett G, Distler JH. Inactivation of tankyrases reduces experimental fibrosis by inhibiting canonical Wnt signalling. Ann Rheum Dis. 2013; 72:1575–1580. [PubMed: 23148305]

Hallmann R, Mayer DN, Berg EL, Broermann R, Butcher EC. Novel mouse endothelial cell surface marker is suppressed during differentiation of the blood brain barrier. Dev Dyn. 1995; 202:325–332. [PubMed: 7626790]

Haseloff RF, Dithmer S, Winkler L, Wolburg H, Blasig IE. Transmembrane proteins of the tight junctions at the blood-brain barrier: structural and functional aspects. Semin Cell Dev Biol. 2015; 38:16–25. [PubMed: 25433243]

Junge HJ, Yang S, Burton JB, Paes K, Shu X, French DM, Costa M, Rice DS, Ye W. TSPAN12 regulates retinal vascular development by promoting Norrin- but not Wnt-induced FZD4/beta-catenin signaling. Cell. 2009; 139:299–311. [PubMed: 19837033]

Klaassen I, Van Noorden CJ, Schlingemann RO. Molecular basis of the inner blood-retinal barrier and its breakdown in diabetic macular edema and other pathological conditions. Prog Retin Eye Res. 2013; 34:19–48. [PubMed: 23416119]

Knowland D, Arac A, Sekiguchi KJ, Hsu M, Lutz SE, Perrino J, Steinberg GK, Barres BA, Nimmerjahn A, Agalliu D. Stepwise recruitment of transcellular and paracellular pathways underlies blood-brain barrier breakdown in stroke. Neuron. 2014; 82:603–617. [PubMed: 24746419]

Korn C, Augustin HG. Mechanisms of vessel pruning and regression. Dev Cell. 2015; 34:5–17. [PubMed: 26151903]

Lai MB, Zhang C, Shi J, Johnson V, Khandan L, McVey J, Klymkowsky MW, Chen Z, Junge HJ. TSPAN12 is a Norrin co-receptor that amplifies Frizzled4 ligand selectivity and signaling. Cell Rep. 2017; 19:2809–2822. [PubMed: 28658627]

Lengfeld JE, Lutz SE, Smith JR, Diaconu C, Scott C, Kofman SB, Choi C, Walsh CM, Raine CS, Agalliu I, Agalliu D. Endothelial Wnt/β-catenin signaling reduces immune cell infiltration in multiple sclerosis. Proc Natl Acad Sci USA. 2017; 114:E1168–E1177. [PubMed: 28137846]

Liebner S, Corada M, Bangsow T, Babbage J, Taddei A, Czupalla CJ, Reis M, Felici A, Wolburg H, Fruttiger M, et al. Wnt/beta-catenin signaling controls development of the blood-brain barrier. J Cell Biol. 2008; 183:409–417. [PubMed: 18955553]

Lim RG, Quan C, Reyes-Ortiz AM, Lutz SE, Kedaigle AJ, Gipson TA, Wu J, Vatine GD, Stocksdale J, Casale MS, et al. Huntington's disease iPSC-derived brain microvascular endothelial cells reveal WNT-mediated angiogenic and blood-brain barrier deficits. Cell Rep. 2017; 19:1365–1377. [PubMed: 28514657]

Luhmann UF, Lin J, Acar N, Lammel S, Feil S, Grimm C, Seeliger MW, Hammes HP, Berger W. Role of the Norrie disease pseudoglioma gene in sprouting angiogenesis during development of the retinal vasculature. Invest Ophthalmol Vis Sci. 2005; 46:3372–3382. [PubMed: 16123442]

Mancuso MR, Kuhnert F, Kuo CJ. Developmental angiogenesis of the central nervous system. Lymphat Res Biol. 2008; 6:173–180. [PubMed: 19093790]

Minshall RD, Tiruppathi C, Vogel SM, Niles WD, Gilchrist A, Hamm HE, Malik AB. Endothelial cell-surface gp60 activates vesicle formation and trafficking via G(i)-coupled Src kinase signaling pathway. J Cell Biol. 2000; 150:1057–1070. [PubMed: 10973995]

Obermeier B, Daneman R, Ransohoff RM. Development, maintenance and disruption of the blood-brain barrier. Nat Med. 2013; 19:1584–1596. [PubMed: 24309662]

Paes KT, Wang E, Henze K, Vogel P, Read R, Suwanichkul A, Kirkpatrick LL, Potter D, Newhouse MM, Rice DS. Frizzled 4 is required for retinal angiogenesis and maintenance of the blood-retina barrier. Invest Ophthalmol Vis Sci. 2011; 52:6452–6461. [PubMed: 21743011]

Paolinelli R, Corada M, Ferrarini L, Devraj K, Artus C, Czupalla CJ, Rudini N, Maddaluno L, Papa E, Engelhardt B, et al. Wnt activation of immortalized brain endothelial cells as a tool for generating a standardized model of the blood brain barrier in vitro. PLoS ONE. 2013; 8:e70233. [PubMed: 23940549]

Phng LK, Potente M, Leslie JD, Babbage J, Nyqvist D, Lobov I, Ondr JK, Rao S, Lang RA, Thurston G, Gerhardt H. Nrarp coordinates endothelial Notch and Wnt signaling to control vessel density in angiogenesis. Dev Cell. 2009; 16:70–82. [PubMed: 19154719]

Potente M, Gerhardt H, Carmeliet P. Basic and therapeutic aspects of angiogenesis. Cell. 2011; 146:873–887. [PubMed: 21925313]

Shimomura Y, Agalliu D, Vonica A, Luria V, Wajid M, Baumer A, Belli S, Petukhova L, Schinzel A, Brivanlou AH, et al. APCDD1 is a novel Wnt inhibitor mutated in hereditary hypotrichosis simplex. Nature. 2010; 464:1043–1047. [PubMed: 20393562]

Stahl A, Connor KM, Sapieha P, Chen J, Dennison RJ, Krah NM, Seaward MR, Willett KL, Aderman CM, Guerin KI, et al. The mouse retina as an angiogenesis model. Invest Ophthalmol Vis Sci. 2010; 51:2813–2826. [PubMed: 20484600]

Stan RV, Kubitza M, Palade GE. PV-1 is a component of the fenestral and stomatal diaphragms in fenestrated endothelia. Proc Natl Acad Sci USA. 1999; 96:13203–13207. [PubMed: 10557298]

Stan RV, Tse D, Deharvengt SJ, Smits NC, Xu Y, Luciano MR, McGarry CL, Buitendijk M, Nemani KV, Elgueta R, et al. The diaphragms of fenestrated endothelia: gatekeepers of vascular permeability and blood composition. Dev Cell. 2012; 23:1203–1218. [PubMed: 23237953]

Stenman JM, Rajagopal J, Carroll TJ, Ishibashi M, McMahon J, McMahon AP. Canonical Wnt signaling regulates organ-specific assembly and differentiation of CNS vasculature. Science. 2008; 322:1247–1250. [PubMed: 19023080]

Sun JF, Phung T, Shiojima I, Felske T, Upalakalin JN, Feng D, Kornaga T, Dor T, Dvorak AM, Walsh K, Benjamin LE. Microvascular patterning is controlled by fine-tuning the Akt signal. Proc Natl Acad Sci USA. 2005; 102:128–133. [PubMed: 15611473]

Takahashi M, Fujita M, Furukawa Y, Hamamoto R, Shimokawa T, Miwa N, Ogawa M, Nakamura Y. Isolation of a novel human gene, APCDD1, as a direct target of the beta-Catenin/T-cell factor 4 complex with probable involvement in colorectal carcinogenesis. Cancer Res. 2002; 62:5651–5656. [PubMed: 12384519]

Tiruppathi C, Naqvi T, Wu Y, Vogel SM, Minshall RD, Malik AB. Albumin mediates the transcytosis of myeloperoxidase by means of caveolae in endothelial cells. Proc Natl Acad Sci USA. 2004; 101:7699–7704. [PubMed: 15136724]

Tran KA, Zhang X, Predescu D, Huang X, Machado RF, Göthert JR, Malik AB, Valyi-Nagy T, Zhao YY. Endothelial β-catenin signaling is required for maintaining adult blood-brain barrier integrity and central nervous system homeostasis. Circulation. 2016; 133:177–186. [PubMed: 26538583]

Turakainen H, Saarimäki-Vire J, Sinjushina N, Partanen J, Savilahti H. Transposition-based method for the rapid generation of gene-targeting vectors to produce Cre/Flp-modifiable conditional knock-out mice. PLoS ONE. 2009; 4:e4341. [PubMed: 19194496]

Wang Y, Rattner A, Zhou Y, Williams J, Smallwood PM, Nathans J. Norrin/Frizzled4 signaling in retinal vascular development and blood brain barrier plasticity. Cell. 2012; 151:1332–1344. [PubMed: 23217714]

Xia CH, Yablonka-Reuveni Z, Gong X. LRP5 is required for vascular development in deeper layers of the retina. PLoS ONE. 2010; 5:e11676. [PubMed: 20652025]

Xu Q, Wang Y, Dabdoub A, Smallwood PM, Williams J, Woods C, Kelley MW, Jiang L, Tasman W, Zhang K, Nathans J. Vascular development in the retina and inner ear: control by Norrin and Frizzled-4, a high-affinity ligand-receptor pair. Cell. 2004; 116:883–895. [PubMed: 15035989]

Ye X, Wang Y, Cahill H, Yu M, Badea TC, Smallwood PM, Peachey NS, Nathans J. Norrin, frizzled-4, and Lrp5 signaling in endothelial cells controls a genetic program for retinal vascularization. Cell. 2009; 139:285–298. [PubMed: 19837032]

Zhao Z, Nelson AR, Betsholtz C, Zlokovic BV. Establishment and dysfunction of the blood-brain barrier. Cell. 2015; 163:1064–1078. [PubMed: 26590417]

Zhou Y, Wang Y, Tischfield M, Williams J, Smallwood PM, Rattner A, Taketo MM, Nathans J. Canonical WNT signaling components in vascular development and barrier formation. J Clin Invest. 2014; 124:3825–3846. [PubMed: 25083995]

Zhou Y, Williams J, Smallwood PM, Nathans J. Sox7, Sox17, and Sox18 cooperatively regulate vascular development in the mouse retina. PLoS ONE. 2015; 10:e0143650. [PubMed: 26630461]

Zhu WH, Guo X, Villaschi S, Francesco Nicosia R. Regulation of vascular growth and regression by matrix metalloproteinases in the rat aorta model of angiogenesis. Lab Invest. 2000; 80:545–555. [PubMed: 10780671]

Zuercher J, Fritzsche M, Feil S, Mohn L, Berger W. Norrin stimulates cell proliferation in the superficial retinal vascular plexus and is pivotal for the recruitment of mural cells. Hum Mol Genet. 2012; 21:2619–2630. [PubMed: 22394677]

Highlights

- Apcdd1 is expressed in retinal endothelium during angiogenesis and barrier formation
- *Apcdd1* mutant mice show decreased vessel pruning and precocious barrier maturation
- Apcdd1 overexpression promotes vessel pruning but delays barrier formation
- The Wnt inhibitor Apcdd1 tightly coordinates vascular pruning and barrier maturation

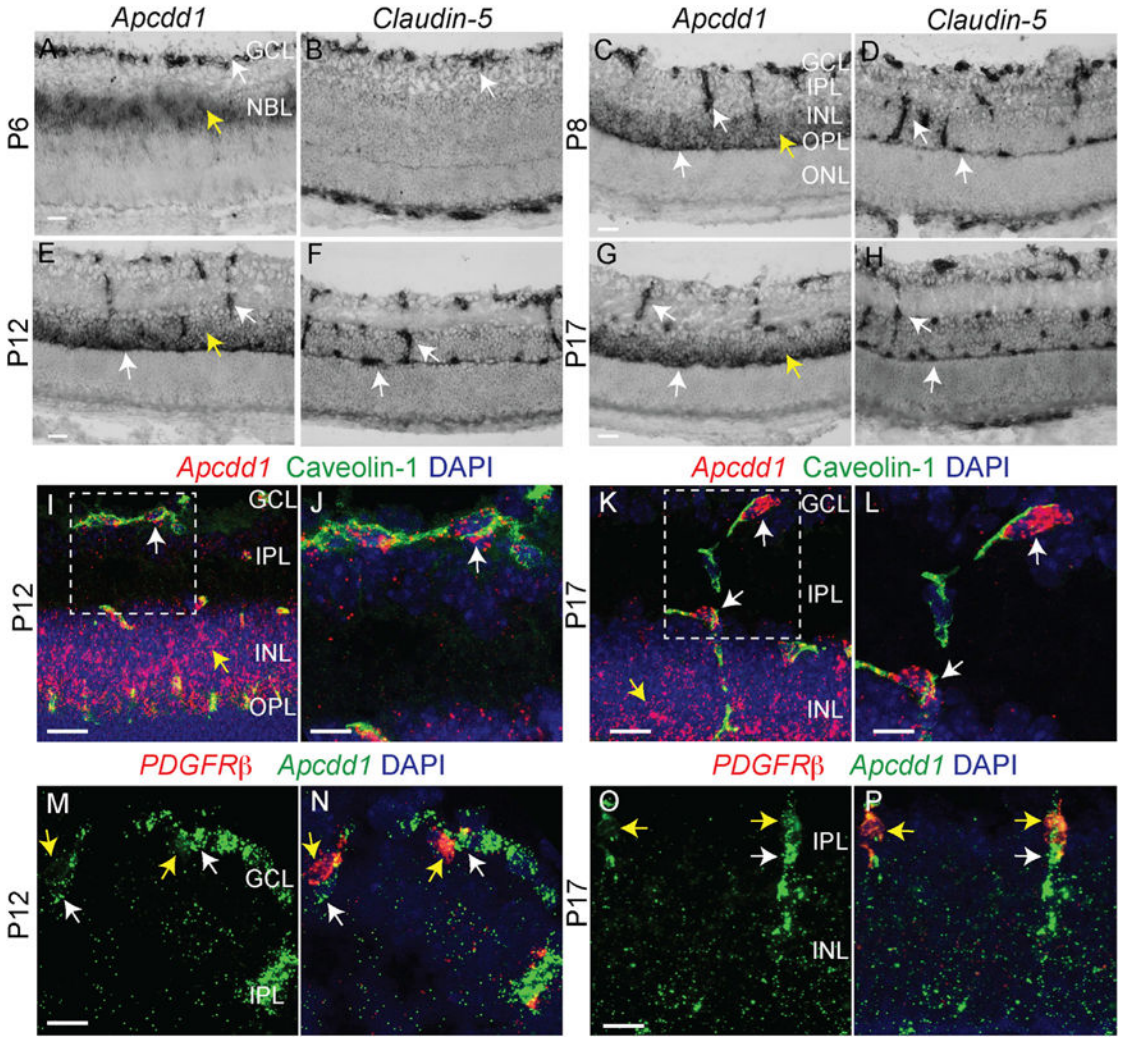

Figure 1. Apcdd1 Is Expressed in Retinal Blood Vessels during Angiogenesis and Blood-Retina Barrier Formation

(A–H) Representative images of RNA *in situ* hybridizations for *Apcdd1* and *Claudin-5* in sections of P6 (A and B), P8 (C and D), P12 (E and F), and P17 (G and H) wild-type mouse retinas (n = 3 mice per time point). *Apcdd1* is expressed by blood vessels in superficial and deep plexi (white arrows), as well as by neural progenitors/neurons (yellow arrows) in the NBL and INL.

(I–L) Fluorescent RNA *in situ* hybridization for *Apcdd1* and immunohistochemistry for Caveolin-1, an EC marker, in P12 (I and J) and P17 (K and L) wild-type retinas (n = 3 mice/time point). *Apcdd1* colocalizes with Caveolin-1, indicating expression in the endothelium (I–L; white arrows). (J and L) Higher magnification of boxed regions in (I) and (K), respectively.

(M–P) Double fluorescent RNA *in situ* hybridization for *Apcdd1* (M and O, green) and merged panels (N and P; *Apcdd1* green and *PDGRF*β red) in P12 (M and N) and P17 (O and P) wild-type retinas. *Apcdd1* colocalizes with Caveolin-1 but very little with PDGFRβ, indicating expression in the endothelium (I–P; white arrows) but not pericytes (M–P; yellow

arrows). *Apcdd1* mRNA is also expressed by non-endothelial cells within the INL (I and K; yellow arrows).

Scale bars represent 50 μm in (A)–(H), 25 μm in (I), (K), and (M)–(P), and 15 μm in (J) and (L). GCL, ganglion cell layer; IPL, inner plexiform layer; NBL, neuroblast layer; OPL, outer plexiform layer; ONL, outer nuclear layer.

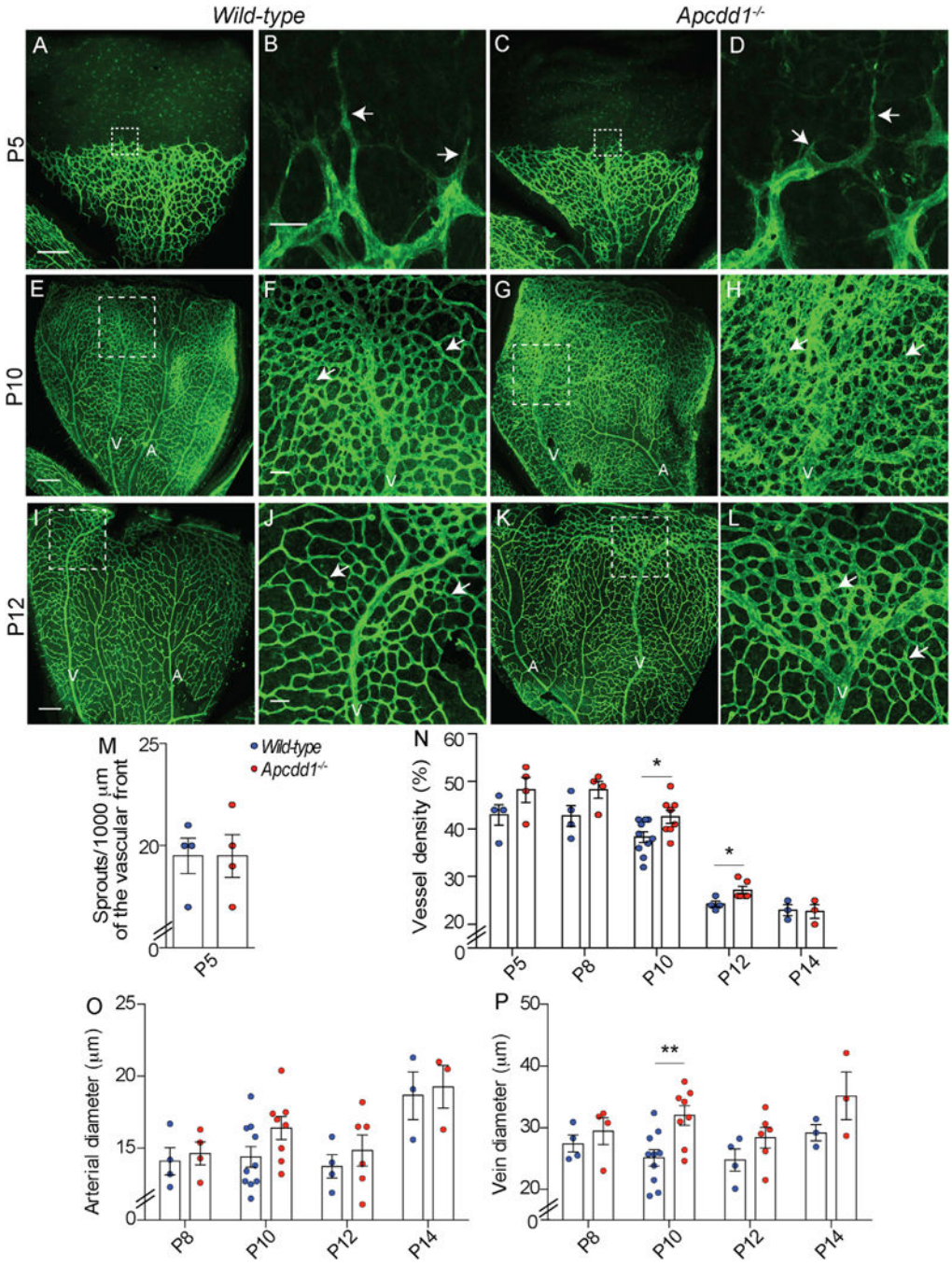

Figure 2. Loss of *Apcdd1* Function Transiently Increases Vessel Density

(A–D) Immunohistochemistry for BSL-FITC (vessel marker) in wild-type and *Apcdd1*$^{-/-}$ P5 retinas. (A) Wild-type and (C) *Apcdd1*$^{-/-}$ retinas show comparable sprouting patterns at the leading edge of the leaflet. (B and D) Higher magnification of boxed regions in (A) and (C), respectively, illustrating sprouting ECs (white arrows).

(E–L) P10 and P12 whole-mount retinas from both genotypes stained for BSL-FITC. *Apcdd1*$^{-/-}$ retinas (G) and (K) have an increased vessel density in perivenous capillaries

compared to wild-type controls (E and I). (F, H, J, and L) Higher magnification of boxed regions in (E), (G), (I), and (K), respectively.

(M) Quantification of sprouts at vascular fronts for wild-type and *Apcdd1*$^{-/-}$ retinas at P5 (n = 4 animals/group).

(N) Quantification of vessel densities in the superficial plexus of wild-type and *Apcdd1*$^{-/-}$ mice from P5 to P14 (n = 3–10 animals/group). *Apcdd1* mutants have a transient increase in vessel density at P10 and P12.

(O and P) Quantification of artery (O) and vein (P) diameters for wild-type and *Apcdd1*$^{-/-}$ mice aged P8 to P14 (n = 3–10 animals/group). *Apcdd1* mutants show increased venous diameters at P10 (P).

Scale bars represent 200 μm in (A), (E), and (I), 50 μm in (F) and (J), and 25 μm in (B). A, artery; V, vein. Data are presented as mean ± SEM, *p < 0.05 **p < 0.01, Student's unpaired t test.

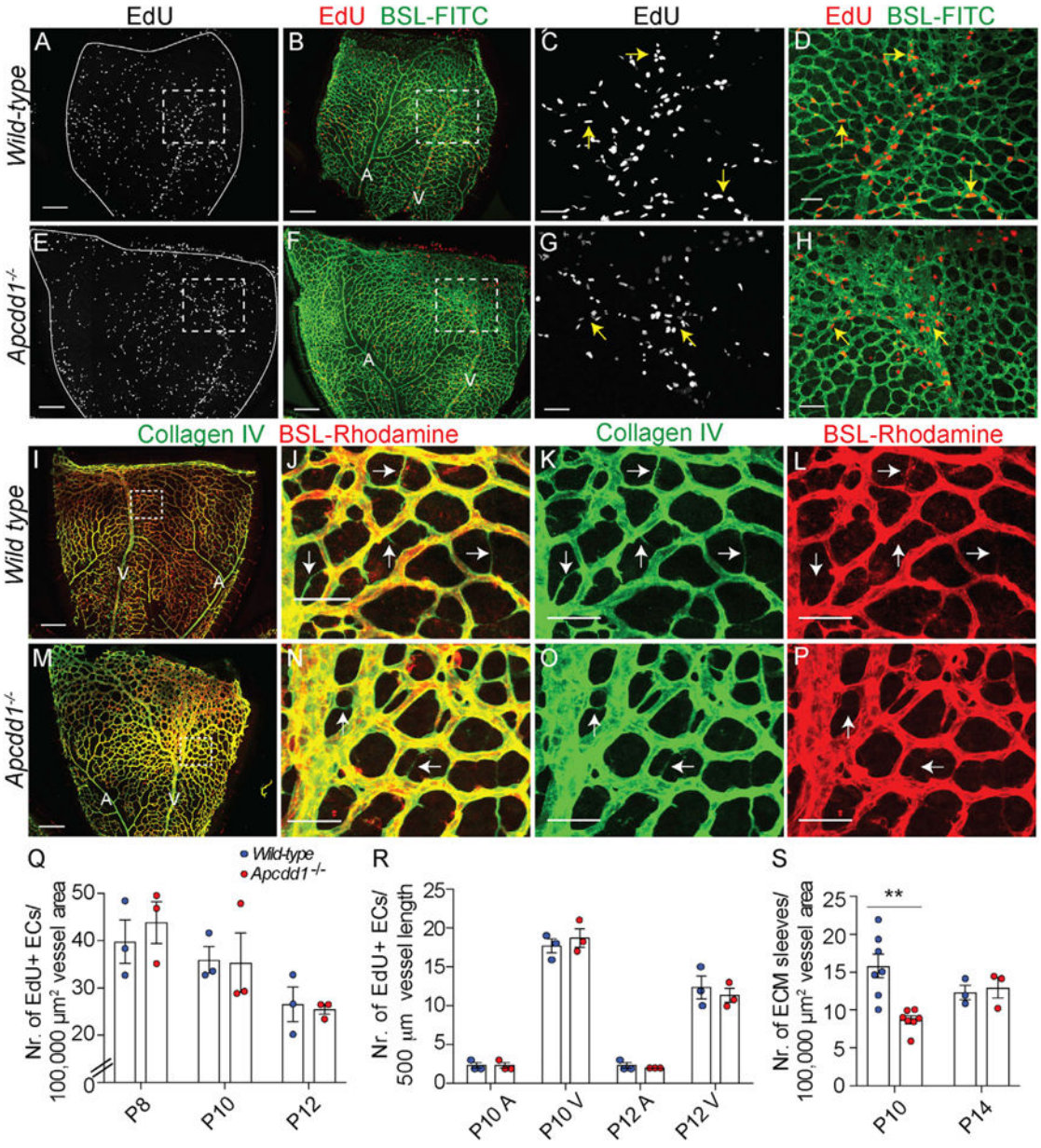

Figure 3. Loss of *Apccd1* Function Reduces Vessel Pruning

(A–H) Immunofluorescence for BSL-FITC and EdU in whole-mount retinas from wild-type littermates and *Apcdd1*$^{-/-}$ mice. Representative images for EdU^{+} ECs (C, D, G, and H; yellow arrows) in P10 wild-type (A–D) and *Apcdd1*$^{-/-}$ (E–H) retinas. (C, D, G, and H) Higher magnification of boxed regions in (A), (B), (E), and (F), respectively.

(I–P) Immunofluorescence for BSL-rhodamine and Collagen IV in whole-mount P10 retinas from wild-type (I–L) and *Apcdd1*$^{-/-}$ (M–P) mice. Empty matrix sleeves (J–L and N–P; white arrows) are defined as Collagen IV^{+} (green) and BSL-rhodamine^{-} (red). (J, L, N, and P). Higher magnification of boxed regions in (I) and (M), respectively.

(Q) Quantification of EdU^{+} ECs per vessel area (n = 3 animals/group).

(R) Quantification of arterial and venous EdU^{+} ECs per vessel length (n = 3 animals/group). *Apcdd1*$^{-/-}$ mice have normal EC proliferation.

(S) Quantification of empty matrix sleeves per vessel area at P10 and P14 (n = 3–7 animals per group). *Apcdd1*$^{-/-}$ retinas have fewer empty matrix sleeves as compared to wild-type. Scale bars represent 200 μm in (A) and (I), 50 μm in (D), and 25 μm in (J). Data are presented as mean ± SEM, **p < 0.01, Student's unpaired t test.

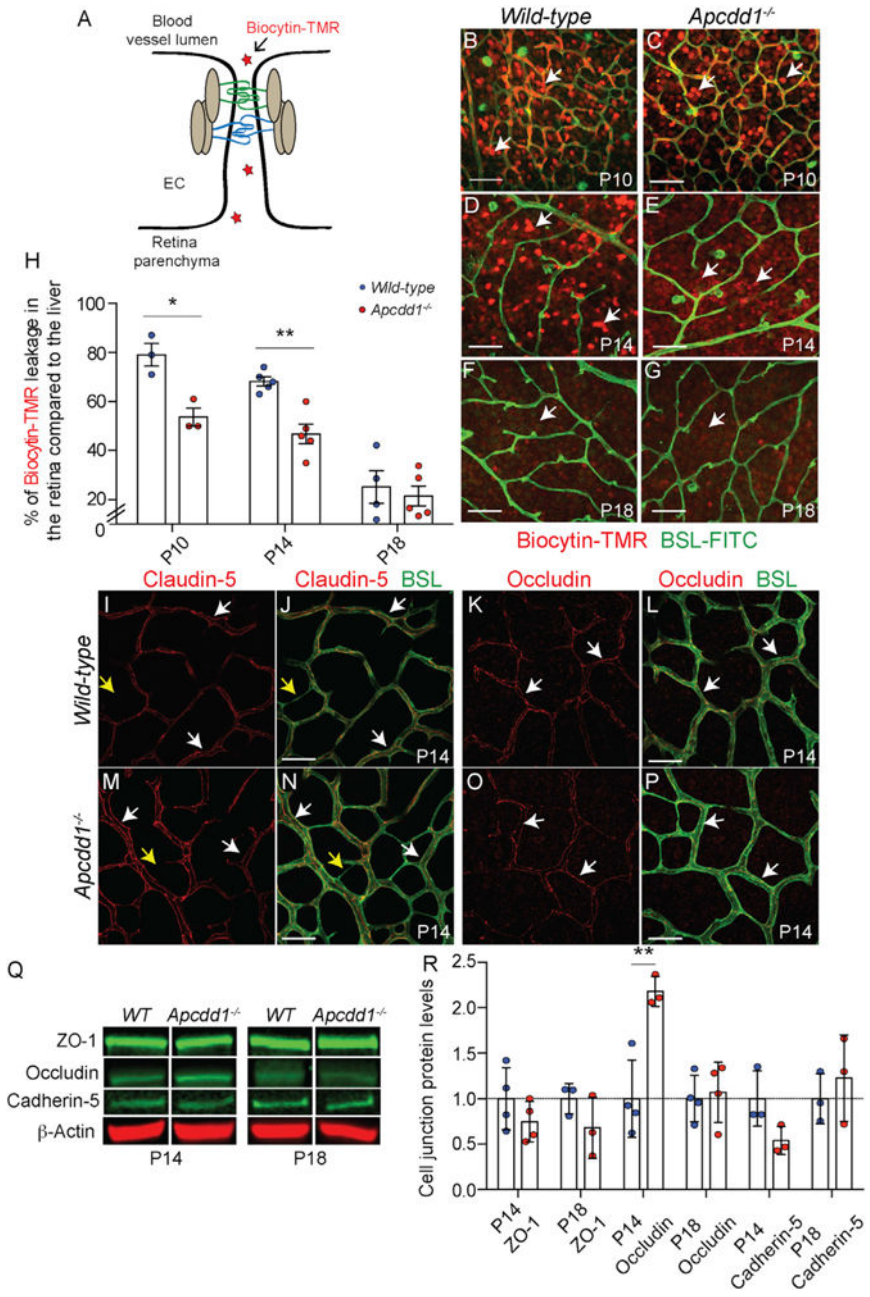

Figure 4. Loss of *Apcdd1* Function Decreases Paracellular BRB Permeability

(A) Diagram for measuring paracellular permeability via leakage of biocytin tetramethylrhod-amine (TMR).

(B–G) Representative images of wild-type (B, D, and F) and *Apcdd1*$^{-/-}$ (C, E, and G) retinas at P10, P14, and P18 following injection of biocytin-TMR. Tracer leakage appears as intense bright puncta in the retinal parenchyma (B–G; white arrows). *Apcdd1*$^{-/-}$ retinas exhibit less tracer leakage at P10 and P14 compared to wild-type controls.

(H) Quantitation of signal intensities for biocytin-TMR leakage outside the retinal vasculature, normalized to the liver (n = 3–5 animals/group). More tracer leakage is seen in wild-type compared to *Apcdd1*$^{-/-}$ retinas at P10 and P14.

(I–P) Immunofluorescence images for Claudin-5 (I and M; red), Claudin-5 (red) and BSL (green) (J and N), Occludin (K and O; red), and Occludin (red) and BSL (green) (L and P) in the superficial plexi of the wild-type and *Apcdd1*$^{-/-}$ retinas at P14. Claudin-5 and Occludin are localized to cell junctions in both genotypes (I–P; white arrows). Note the absence of Claudin-5 in regressing vessels (I, J, M, and N; yellow arrows).

(Q) Western blot analysis for TJ proteins ZO-1 and Occludin and adherens junction protein Cadherin-5 in P14 and P18 retinal lysates.

(R) Quantification of ZO-1, Occludin, and Cadherin-5 protein levels using LICOR. At P14, *Apcdd1*$^{-/-}$ retina lysates show a dramatic increase in Occludin (n = 3–4 replicates/group). Scale bar represents 50 μm in (B)–(G). Data in (H) are presented as mean ± SEM, whereas in (R) as mean ± SD; *p < 0.05. **p < 0.01, Student's unpaired t test.

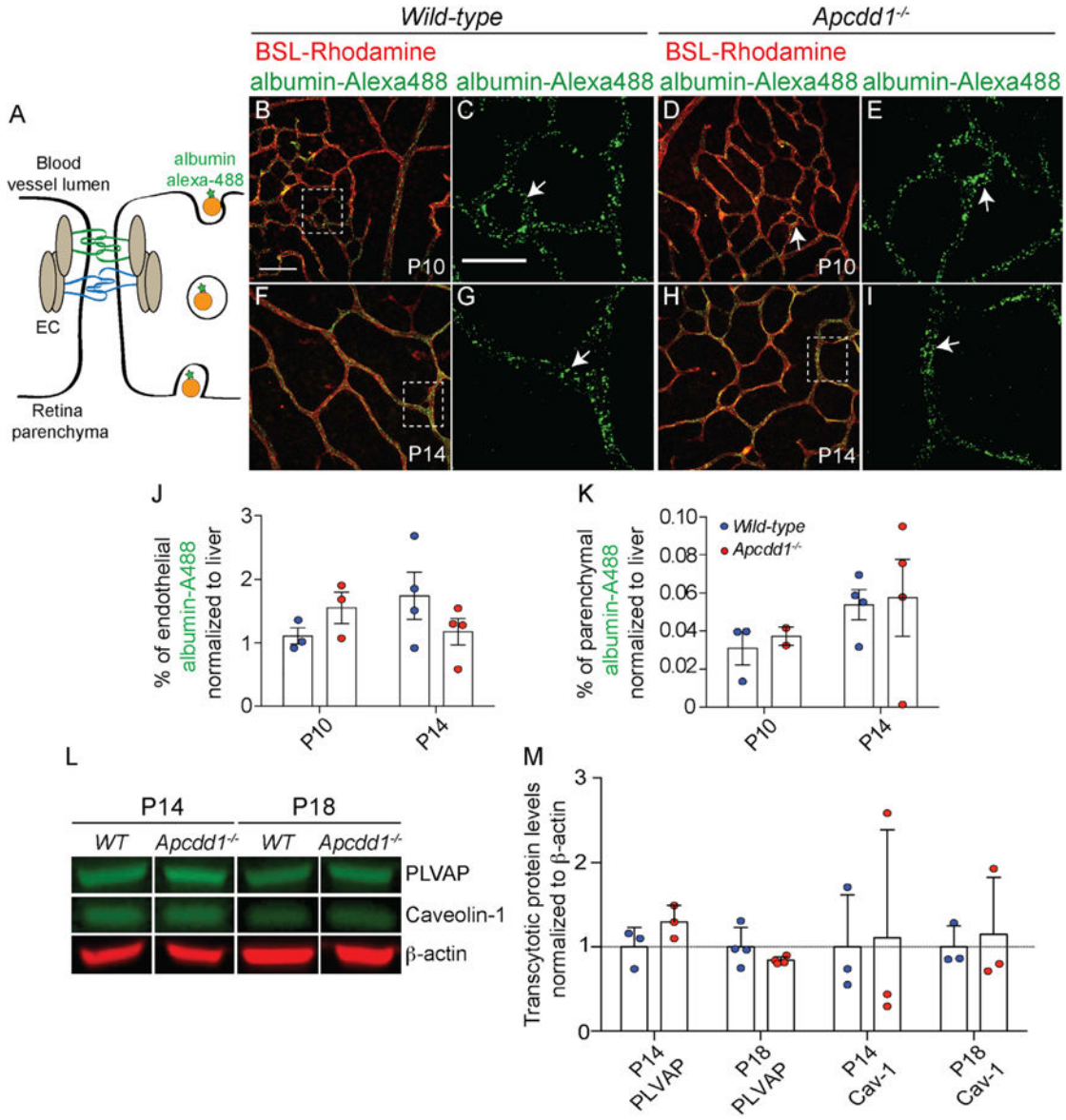

Figure 5. Transcellular BRB Permeability Is Unaffected in *Apcdd1* Mutants

(A) Diagram outlining albumin endocytosis in retinal ECs.

(B–I) Representative images of wild-type (B, C, F, and G) and *Apcdd1*$^{-/-}$ (D, E, H, and I) retinas at P10 and P14 following injection of albumin-Alexa Fluor 488. *Apcdd1*$^{-/-}$ retinas have normal albumin uptake compared to wild-type retinas at both stages (C, E, G, and I; white arrows).

(J and K) Quantification of intra-endothelial (J) and parenchymal (K) albumin normalized to liver (n = 3–4 animals/group).

(L and M) Western blot analysis (L) and quantification (M) for Caveolin-1 and PLVAP (n = 3–4 replicates/group). *Apcdd1*$^{-/-}$ retinal lysates have no significant differences in Caveolin-1 and PLVAP levels.

Scale bars represent 50 μm in (B) and 25 μm in (C). Data in (J) and (K) are presented as mean ± SEM, and in (M) as mean ± SD; Student's unpaired t test.

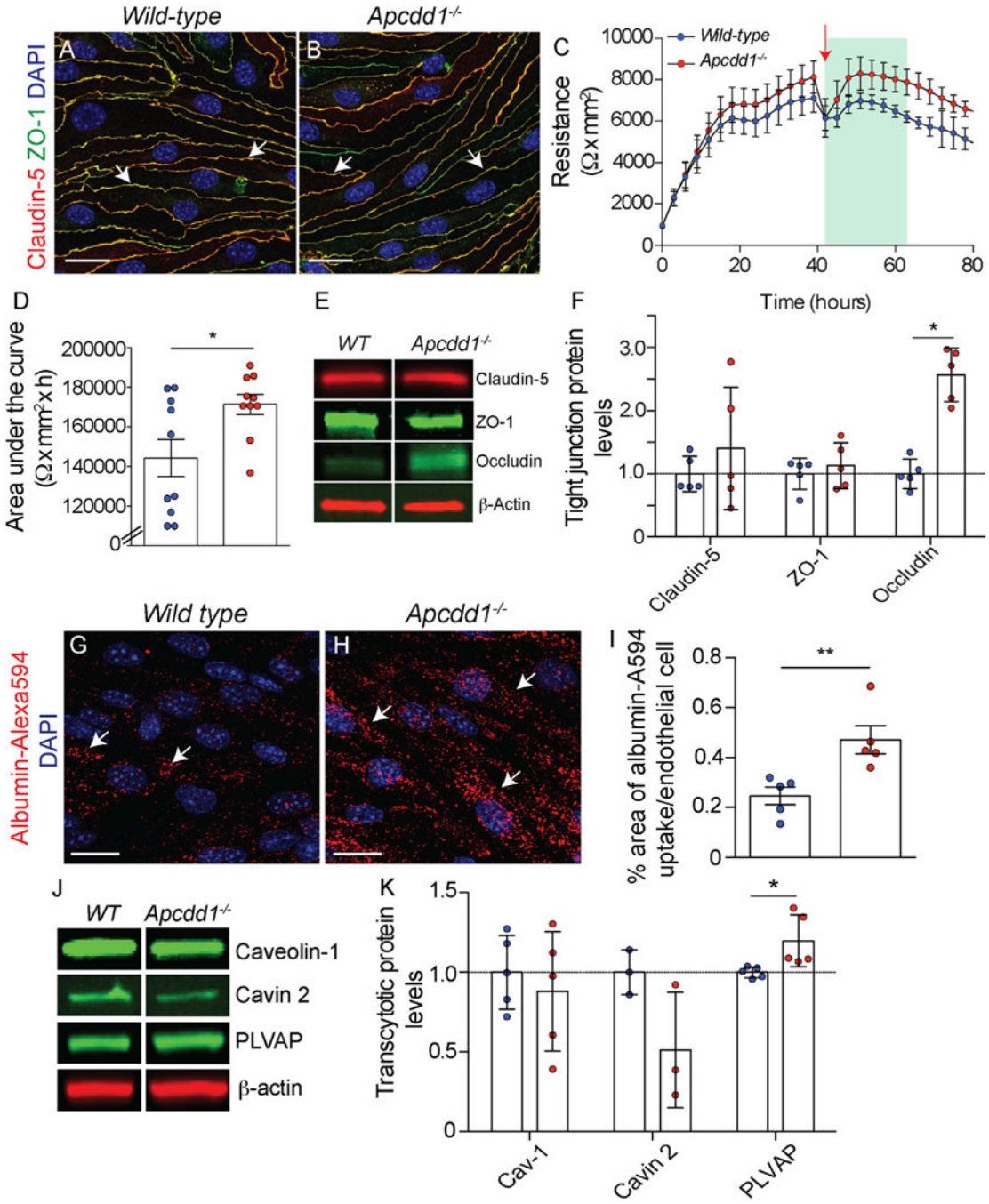

Figure 6. *Apcdd1*$^{-/-}$ Brain ECs Display Decreased Paracellular but Increased Transcellular Permeability *In Vitro*

(A and B) Immunofluorescence for Claudin-5 and ZO-1 in wild-type (A) and *Apcdd1*$^{-/-}$ (B) BECs. There is no detectable difference in junctional localization for either protein in wild-type or *Apcdd1*$^{-/-}$ BECs. (A and B; white arrows).

(C) Graph of trans-endothelial electrical resistance (TEER) in monolayers of wild-type or *Apcdd1*$^{-/-}$ BECs. Green area indicates the period of TEER measurement after incubation in low serum (1%) media (red arrow indicates start of TEER measurement).

(D) Quantitation of the areas under the curve for the green region depicted in (C) (n = 10 independent experiments). *Apcdd1*$^{-/-}$ BECs show increased TEER compared to wild-type BECs.

(E and F) Western blot and quantification for Claudin-5, ZO-1, and Occludin in wild-type and *Apcdd1*$^{-/-}$ BECs. *Apcdd1*$^{-/-}$ BECs have increased Occludin expression (n = 5 independent experiments).

(G and H) Distribution of albumin-Alexa Fluor 594 puncta in wild-type (G; white arrows) and *Apcdd1*$^{-/-}$ (H; white arrows) BECs following incubation to measure transcellular permeability.

(I) Quantification of EC-associated albumin in wild-type and *Apcdd1*$^{-/-}$ BECs. *Apcdd1*$^{-/-}$ BECs have a significant increase in albumin uptake (n = 5 independent experiments).

(J and K) Western blot (J) and quantitation (K) for Caveolin-1, Cavin-2, and PLVAP (n = 3–5 independent experiments). *Apcdd1*$^{-/-}$ BECs show increased PLVAP expression.

Scale bars represent 15 μm. Data in (D) and (I) are presented as mean ± SEM and in (F) and (K) as mean ± SD; *p < 0.05 **p < 0.01, Student's unpaired t test.

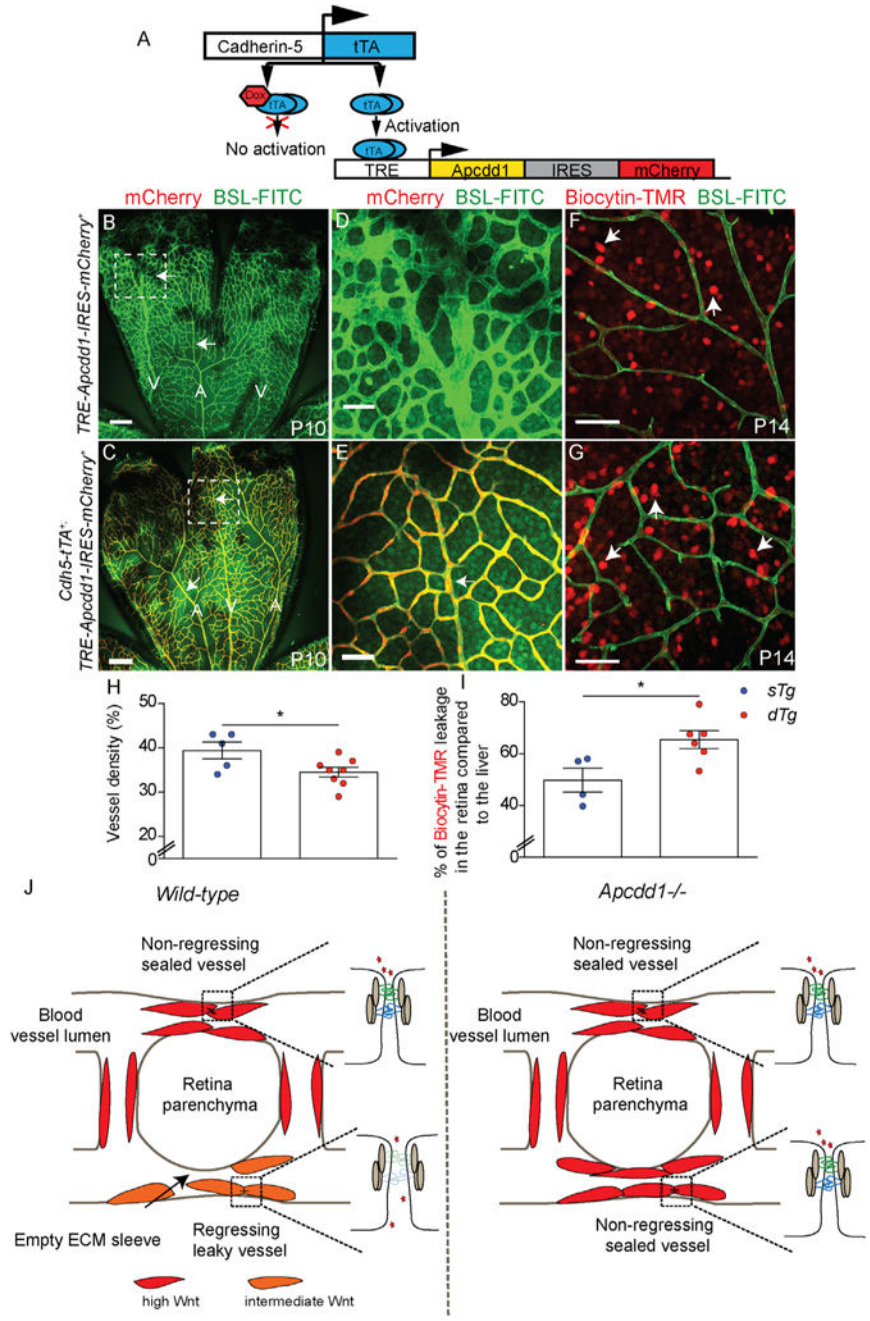

Figure 7. Endothelial Apcdd1 Overexpression Results in Decreased Vessel Density but Delayed Paracellular Barrier Formation in the Retina

(A) Schematic diagram for overexpression of Apcdd1 in ECs.

(B–E) Representative images of BSL-FITC and mCherry expression in *TRE3-Apcdd1-IRES-mCherry*$^{+}$ (sTg) (B and D) and *Cadherin5-tTA*$^{+}$; *TRE3-Apcdd1-IRES-mCherry*$^{+}$ (dTg) (C and E) P10 retinas. mCherry is expressed in the vasculature of dTg (C and E) but not sTg (B and D) animals. (D and E) Higher magnifications of boxed regions in (B) and (C), respectively.

(F and G) Representative images of sTg (F) and dTg (G) retinas at P14 following injection of biocytin-TMR. Tracer leakage appears as intense bright puncta in the retinal parenchyma (F and G; white arrows).

(H) Quantification of vessel densities in the superficial plexus of sTg and dTg P10 retinas (n = 5–8 animals/group). dTg mice have decreased vessel density at P10.

(I) Quantitation of signal intensities for biocytin-TMR leakage outside the retinal vasculature, normalized to the liver (n = 4–6 animals/group). Doubly transgenic retinas show increased tracer leakage compared to singly transgenic retinas at P14.

(J) Diagrams of canonical Wnt signaling activity and tight junction structure in non-regressing sealed vessels and regressing leaky vessels for wild-type and *Apcdd1*$^{-/-}$ retinas. In wild-type mice, Apcdd1 reduces Wnt levels from high (red) to intermediate (orange) in a subset of vessels that will undergo regression. Furthermore, Apcdd1 prevents formation of mature tight junctions (three lines) in vessels destined for regression. In *Apcdd1*$^{-/-}$ retinas, more vessels have high levels of Wnt signaling and thus form a mature barrier but do not undergo regression. Therefore, Apcdd1 precisely sculpts the levels of Wnt activity in retina ECs to coordinate vessel pruning and barrier maturation.

Scale bars represent 200 μm in (B) and (C), 50 μm in (D) and (E), and 25 μm in (F) and (G). sTg, single transgenic; dTg, double transgenic. Data are represented as mean ± SEM; *$p < 0.05$, Student's unpaired t test.